

Taking a Respite from Representation Learning for Molecular Property Prediction

Jianyuan Deng¹, Zhibo Yang², Hehe Wang³, Iwao Ojima³, Dimitris Samaras², and Fusheng Wang^{1,2,*}

¹Stony Brook University, Department of Biomedical Informatics, Stony Brook, 11790, United States

²Stony Brook University, Department of Computer Science, Stony Brook, 11790, United States

³Stony Brook University, Department of Chemistry, Stony Brook, 11790, United States

ABSTRACT

Artificial intelligence (AI) has been widely applied in drug discovery with a major task as molecular property prediction. Despite booming techniques in molecular representation learning, fundamentals underlying molecular property prediction haven't been carefully examined yet. In this study, we conducted a systematic evaluation on a collection of representative models using various molecular representations. In addition to the commonly used MoleculeNet benchmark datasets, we also assembled a suite of opioids-related datasets from ChEMBL and two additional activity datasets from literature. To interrogate the basic predictive power, we also assembled a series of descriptors datasets with varying sizes to evaluate the models' performance. In total, we trained 62,820 models, including 50,220 models on fixed representations, 4,200 models on SMILES sequences and 8,400 models on molecular graphs. We first conducted dataset profiling and highlighted the activity-cliffs issue in the opioids-related datasets. We then conducted rigorous model evaluation and addressed key questions therein. Furthermore, we examined inter-/intra-scaffold chemical space generalization and found that activity cliffs significantly can impact prediction performance. Based on extensive experimentation and rigorous comparison, representation learning models still show limited performance in molecular property prediction in most datasets. Finally, we explored into potential causes why representation learning models fail and highlighted the importance of dataset size. By taking this respite, we reflected on the fundamentals underlying molecular property prediction, the awareness of which can, hopefully, bring better AI techniques in this field.

1 Introduction

Drug discovery is an expensive process in both time and cost with a daunting attrition rate. As revealed by a recent study¹, the average cost of developing a new drug was around 1 billion dollars and has been ever increasing². In the past decade, the practice of drug discovery has been undergoing radical transformations in light of the advancements in artificial intelligence (AI)^{3–5}, which, at its core, is molecular representation learning. Molecules are usually denoted by: 1) fixed representations, such as fingerprints and structural keys, which indicate the existence of certain structural patterns, 2) linear notations, such as Simplified Molecular Input Line Entry System (SMILES) strings and 3) molecular graphs⁶. With the advent of the deep-learning era, various neural networks have been proposed for molecular representation learning, such as convolutional neural networks (CNNs), recurrent neural networks (RNNs) and graph neural networks (GNNs), among others⁵. One major task for AI in drug discovery is molecular property prediction, which seeks to learn a function that maps a structure to a property value. In the literature, deep representation learning has been widely reported to show great potential in molecular property prediction over fixed molecular representations^{7,8}. More recently, to address the lack of labeled data in drug discovery, self-supervised learning has been proposed to leverage large-scale, unlabeled corpus for both SMILES strings^{9–11} and molecular graphs^{12–15}, which has enabled state-of-the-art (SOTA) performance based on the MoleculeNet benchmark datasets¹⁶.

Nevertheless, AI-driven drug discovery is not without its critiques despite its current prosperity. Usually, when a new technique is developed for molecular property prediction, improved metrics by experimenting on the MoleculeNet benchmark datasets¹⁶ are used to substantiate the argument that the model outperforms previous ones. Although novel techniques are indeed proposed along with impressive metrics, most often they do not suffice to solve the molecular property prediction need in real-world drug discovery settings. In fact, the existing practice of representation learning for molecular property prediction can be dangerous yet quite rampant¹⁷. The detailed issues are elaborated as follows.

First, there is a heavy reliance on the MoleculeNet benchmark datasets, which may be of little relevance to real-world drug discovery¹⁸. Moreover, despite the wide adoption of the benchmark datasets, the actual data splits vary in the literature, which entail unfair performance comparison¹⁹. Very often, achieving SOTA performance becomes the major pursuit of new model development, which also leads to little focus on the statistical rigor and the model applicability¹⁷. For instance, when reporting prediction performance for a newly developed model, most papers just used mean values averaged over 3-fold^{7,13,20} or 10-fold^{11,12,19,21} splits. The seeds for dataset splitting may or may not be explicitly provided. Sometimes, it may just come from some arbitrary split with a few individual runs. The inherent variability underlying dataset splitting is simply ignored. The caveat is that, without rigorous analysis, the seemingly improved metric values may

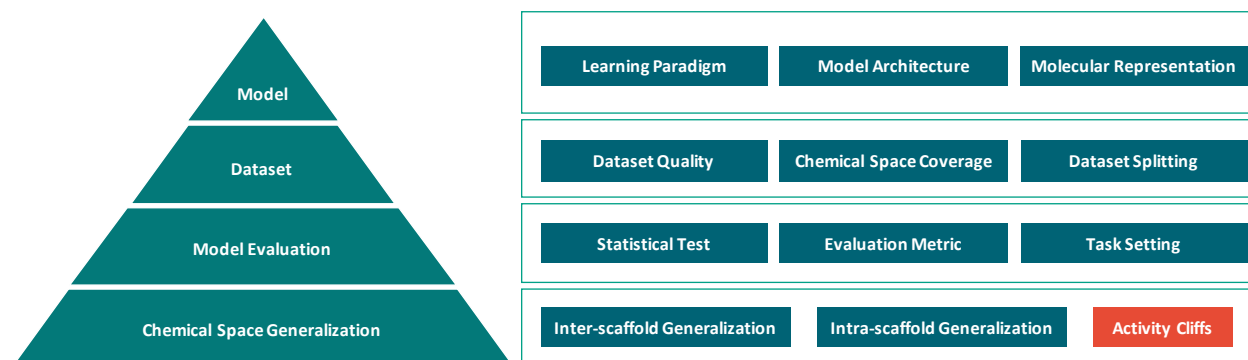


Figure 1. Key Aspects underlying Molecular Property Prediction. There are four aspects underlying molecular property prediction: model, dataset, model evaluation and chemical space generalization. Usually in the literature, the focus is more on the model, which aims at developing novel learning paradigms or model architectures on specific molecular representation formats. However, other aspects, which are pertaining to 1) what the model is built upon, 2) how the model is evaluated and 3) eventually what the model is capable of, should also be considered. For the dataset, its quality (dataset size and label accuracy such as duplicates, contradictories and uncertainty), the chemical space coverage (w.r.t. both structures and labels) and the splitting method should be carefully checked before building a model applicable to a certain property prediction task. For the model evaluation, the use of statistical test, evaluation metric and the task setting also affect the observed prediction performance and may even alter the conclusion. For the chemical space generalization, there is a necessity to clarify what type of generalization the model is capable of and whether the activity-cliffs issue is also addressed.

just be some statistical noise¹⁷. As for model applicability, besides limited relevance of the heavily used MoleculeNet benchmark datasets, there is also a lack of practical relevance for the recommended evaluation metrics. One example is AUROC, which, as opined by Robinson *et al.*¹⁷, cannot well capture the true positive rate, a more relevant metric in virtual screening. To address these existing issues, we took a respite to rethink key aspects underlying molecular property prediction in this study. We conducted a systematic evaluation on representative models in molecular property prediction, with a focus on: 1) dataset profiling, including label distribution and structural analysis; 2) model evaluation, on the molecular representations, statistical test, evaluation metrics and task settings (and label noise); 3) chemical space generalization, w.r.t. inter-scaffold and intra-scaffold generalization. To explain why representation learning models would fail, we applied all models on a series of datasets with varying sizes for the prediction of basic molecular descriptors.

The outline of the paper is as follows. We first discussed the preliminaries for molecular property prediction, including molecular representations, model architectures and learning paradigms⁵. We then discussed in detail the rationale of this study and proposed our experiment schemes. Secondly, we elaborated on the methods, including datasets collection, evaluation metrics, model training and statistical analyses. To further evaluate the usefulness of the molecular representation learning models, we also assembled a suite of opioids-related datasets from ChEMBL²² and a series of datasets on basic molecular descriptors, in addition to the MoleculeNet benchmark datasets, the activity datasets proposed by Bender group²³ and the MoleculeACE datasets²⁴. Thirdly, we presented the results, where we reflected on three major aspects:

1) dataset profiling, 2) model evaluation and 3) chemical space generalization. Finally, we explored why representation learning models would fail and discussed our thoughts on how to advance representation learning for molecular property prediction. By taking this respite, we reflected on the key aspects underlying molecular property prediction, which should be considered in future model development (Figure 1). Similar to the quote from Bender *et al.*^{25,26} “a method cannot save an unsuitable representation which cannot remedy irrelevant data for an ill-thought-through question”, our central thesis is that *“a model cannot save an unqualified dataset which cannot remedy an improper evaluation for an ambiguous chemical space generalization claim”*.

2 Preliminaries

2.1 Molecular representations

2.1.1 Fixed representations

Over the years, various formats have been used to represent small molecules^{5,6}. Arguably, the simplest format are the 1D descriptors which represent a molecule based on its formula, such as atom counts, types and molecular weight. Besides, there are 2D descriptors of a molecule, such as refractivity descriptors and fragment descriptors, which can be computed rapidly by RDKit. For instance, there are 200 molecular features covered by RDKit2D descriptors. Among them, a subset of 11 drug-like PhysChem descriptors, (namely MolWt, MolLogP, NumHDonors, NumHAcceptors, NumRotatableBonds, NumAtoms, NumHeavyAtoms, MolMR, PSA, FormalCharge and NumRings), can also be used for prediction²⁴. The normalized RDKit2D descriptors can be concatenated with the learned representations, as proposed in Chemprop^{8,13}.

Table 1. Fixed Molecular Representations

Type	Name	Dimension
Descriptors	RDKit2D	200
Descriptors	PhysChem	11
Structural Keys	MACCS	2048
Fingerprints	MorganBits	2048
Fingerprints	MorganCounts	2048
Fingerprints	AtomPairs	2048

Moreover, molecules can also be represented by 2D fingerprints, including 1) structural keys, such as Molecular ACCess System (MACCS) keys and 2) path-based or circular fingerprints²⁷. The circular fingerprints can be either 1) bit vectors, which are binary vectors with each dimension tracking the presence or absence of a particular substructure or 2) count vectors, which track the frequency of each substructure. One of the most widely used circular fingerprints is the extended-connectivity fingerprints (ECFP) based on the Morgan algorithm, firstly proposed to solve the molecular isomorphism issue, which is to identify if two molecules, with different atom numberings, are the same^{28,29}. There are three sequential stages during ECFP generation: 1) an initial assignment stage when each atom has an integer identifier assigned, 2) an iterative updating stage when each atom identifier is updated to reflect the identifiers of each atom’s neighbors, including identification of whether it is a structural duplicate of other features, 3) a duplicate identifier removal stage when multiple occurrences of the same feature are reduced to a single representative in the final feature list, which generates the standard MorganBits fingerprints. Notably, the occurrence count may be retained if a set of counts are required, which correspond to the MorganCounts fingerprints. ECFP has been the de facto standard circular fingerprint and is still valuable in drug discovery²⁷. The vector size of ECFP is usually 1024 or 2048. The radius size of ECFP can either be 2 or 3, corresponding to ECFP4 and ECFP6, which are common variants of ECFP in the literature. For instance, Yang *et al.*⁸ used ECFP4 while Mayr *et al.*⁷, Robinson *et al.*¹⁷ and Skinnider *et al.*³⁰ used ECFP6. In this study, we compared ECFP with different vector and radius sizes. More recently, atom-pair fingerprints have been proposed to capture the size and shape of a molecule³¹, which is also evaluated here. The list of fixed molecular representations are summarized in Table 1.

2.1.2 Molecular graphs

Intuitively, small molecules can be represented as graphs, with atoms as nodes and bonds as edges. Formally, a graph is defined as $G = (V, E)$, where V and E represent nodes (atoms) and edges (bonds), respectively. The attributes of atoms can be represented by a node feature matrix X and each node v can be represented by an initial vector $x_v \in R^D$ and a hidden vector $h_v \in R^D$. Similarly, the attributes of bonds can also be represented by a feature matrix. In addition, an adjacency matrix A is used to represent the pairwise connections between

Table 2. Commonly Used Node and Edge Features

Type	Feature	Notes
Node	Atom type	Element type
Node	Formal charge	Assigned charges
Node	Implicit Hs	Number of bonded hydrogens
Node	Chirality	<i>R</i> or <i>S</i> configuration
Node	Hybridization	Orbital hybridization
Node	Aromaticity	Aromatic atom or not
Edge	Bond type	Single, double, triple, aromatic
Edge	Conjugated	Conjugated or not
Edge	Stereoisomers	cis or trans (<i>E</i> or <i>Z</i>), none, any

nodes. For every two nodes v_i and v_j , $A_{ij} = 1$ if there is a bond connecting nodes v_i and v_j ; $A_{ij} = 0$ otherwise. Usually, the edge feature matrix and the adjacency matrix can be combined to form an adjacency tensor. Table 2 summarizes the commonly used node and edge features.

2.1.3 SMILES strings

Although the graph representation carries more structural information, one drawback is that graphs are often storage- and memory-demanding⁶. Alternatively, a more computationally efficient representation of molecules is the SMILES strings³², where atoms are represented by the atomic symbols and bonds by symbols like "-", "=", "#", and ":", corresponding to single, double, triple and aromatic bonds, respectively. Notably, single bonds and aromatic bonds are usually omitted. Moreover, parentheses are used to denote the branches in a molecule. For the cyclic structure, a single or aromatic bond is first broken down in the ring and the bonds are then numbered in any order with the ring-opening bonds by a digit following the atomic symbol at each ring. Notably, one molecule can have multiple SMILES-string representations⁶. Thus, the canonicalized SMILES strings³³ are more often used. To be machine-readable, SMILES strings should be firstly tokenized and the tokens are then converted into one-hot vectors.

2.2 Model architectures

So far, various model architectures have been proposed for molecular property prediction, such as RNNs, GNNs and transformers⁵. Originally designed for handling sequential data (e.g., text and audio), RNNs can be naturally used to model molecules formatted as the SMILES strings, such as SMILES2Vec³⁴ and SmilesLSTM⁷. GNNs, on the other hand, can be applied on the molecular graphs, such as graph convolutional networks (GCN)³⁵, graph attention network (GAT)³⁶, message passing neural networks (MPNN)³⁷, directed MPNN (D-MPNN)⁸, graph isomorphism networks (GIN)^{12,38}. To address the lack of annotated data in drug discovery, self-supervised learning has recently been proposed for pretraining on large-scale unlabeled molecules corpus before downstream finetuning⁵. Here, we mainly utilized two self-supervised models: MolBERT¹¹ and GROVER¹³, which use SMILES strings and molecular graphs as input, respectively. To eval-

uate the effectiveness of advanced molecular representation learning models, we used traditional machine learning models on fixed molecular representations as baselines.

2.2.1 Traditional ML models: RF, XGBoost & SVM

RF (Random Forest) is an ensemble of decision tree predictors, which can be applied for classification and regression tasks³⁹. RF has been widely adopted in drug discovery prior to the "deep-learning" era⁴. XGBoost (eXtreme Gradient Boosting) is also a popular ensemble learning model⁴⁰. Different from RF which builds multiple decision trees independently, XGBoost iteratively trains decision trees to correct the errors of previous trees, which is achieved by adding a new tree to the model that focuses on the samples that were not correctly predicted by the previous ones. XGBoost is computationally efficient and can handle large datasets, making it a suitable option for many real-world applications. SVM (Support Vector Machine) is a classical ML model for both classification and regression tasks⁴¹, which is based on the concept of finding the optimal hyperplane that separates different classes in a dataset. SVM has been successfully applied in various domains, including image recognition and text classification, especially in low-data regimes. Previous studies have shown that RF, XGBoost and SVM establish strong baselines for deep learning models in molecular property prediction⁴². Therefore, we selected them as baselines for evaluating the advanced molecular representation learning models.

2.2.2 Sequence-based models: RNN & MolBERT

The SMILES strings can be viewed as a "chemical" language. Language models, therefore, have been widely applied in molecular representation learning for molecular property prediction, molecule generation and retro-synthesis prediction⁵. Related model architectures include RNNs and Transformers. In this study, we evaluated GRU⁴³ (a RNN variant) and MolBERT¹¹ (a Transformer-based model), both of which are sequence-based models. GRU, like other RNNs, is designed to process sequential data and has shown to be particularly effective in natural language processing (NLP) tasks, such as language modeling and machine translation⁴⁴. Recently, inspired by Bidirectional Encoder Representation from Transformers (BERT) in natural language processing⁴⁵, Fabian *et al.*¹¹ exploited the architecture of BERT for molecular property prediction. Using Transformers as the building block, MolBERT is pretrained on a corpus of c.a. 1.6M SMILES strings, which improves prediction performance on 6 benchmark datasets in both classification (BACE, BBBP, HIV) and regression (ESOL, FreeSolv, Lipop) settings¹⁶.

The abstracted architecture of MolBERT is depicted in Figure 2. An input SMILES string is firstly tokenized and embedded into a sequence of d -dimensional vectors. Unlike RNNs, which handle the input sequentially, a positional embedding layer is added to the input tokens to capture the sequential information. A stack of n BERT encoder layers is then added on top of the embedding layers to learn the latent representations of the input sequence. During pretraining, dif-

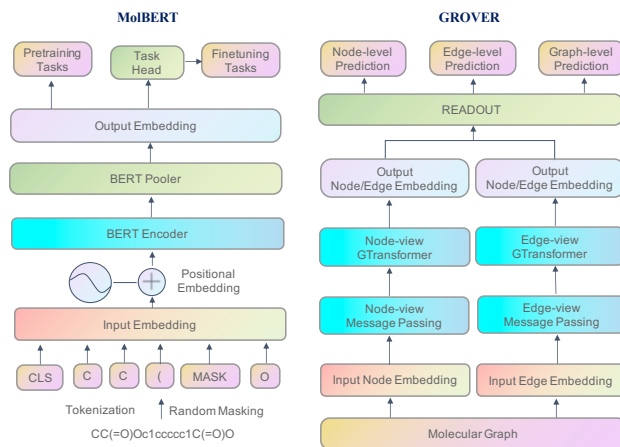


Figure 2. Abstracted Model Architectures Modified from MolBERT¹¹ and GROVER¹³.

ferent pretext self-supervised tasks, such as masked language modeling, are designed to utilize the output embeddings after the pooler layer. During finetuning, new task heads can be appended by attaching a single linear layer to the pooled output for downstream property prediction. The learned weights of the backbone model during pretraining are fixed, which provide a better model initialization and can also reduce training burden during finetuning, especially when the model is large.

MolBERT is pretrained on a vocabulary of 42 tokens and a maximum sequence length of 128 characters. To support arbitrary length of SMILES strings at inference (for instance, we adopted the maximum sequence length of 400 during finetuning), relative positional encoding is used⁴⁶. Following the original BERT model, MolBERT uses the BERTBase architecture with an output embedding size of 768, 12 BERT encoder layers, 12 attention heads and a hidden size of 3,072, resulting in c.a. 85M parameters. The pretrained MolBERT, with backbone weights frozen, plus one linear layer is used here, which results in 769 parameters to fit during finetuning.

2.2.3 Graph-based models: GCN, GIN & GROVER

As stated in Section 2.1.2, molecules can be intuitively abstracted as graphs. GNNs, therefore, have also been widely applied in molecular representations learning⁵. The core operation in GNNs is message passing, a.k.a. neighborhood aggregation³⁷. During message passing, a node's hidden state is iteratively updated by aggregating the hidden states of its neighboring nodes and edges, which involves multiple hops. After each iteration, the message vectors can be integrated using certain AGGREGATE functions, such as sum, mean, max pooling or graph attention⁴⁷. The AGGREGATE function is essentially a trainable layer, which is shared by different hops within an iteration. When the message passing is completed, the hidden states of the last hop from the last iteration are used as the nodes' embeddings, followed by a READOUT function to obtain the graph-level embedding. Among different variants of GNNs, GCN³⁵ is a basic type that encodes the molecular

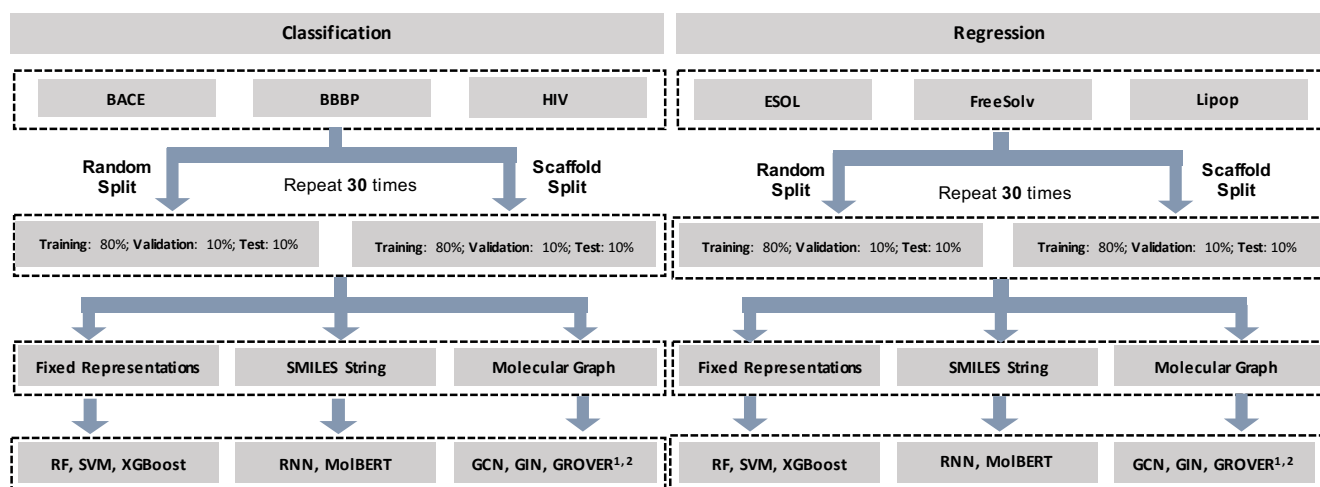


Figure 3. Experiment Scheme in the MoleculeNet Benchmark Datasets. (GROVER^{1,2}: GROVER, GROVER_RDKit)

structure into a graph and then applies convolutional operations to extract features. GIN³⁸ further improves GCN with a permutation-invariant aggregation operation, which ensures the learned embeddings invariant to the node orderings. This allows GIN to handle graph isomorphism, where two graphs have the same structure but different node labels.

To improve prediction performance in low-data regimes, pretraining has also been proposed for GNNs with common tasks as¹²: 1) self-supervised node-level atom type prediction and 2) supervised graph-level molecular label prediction. However, supervised pretraining may cause "negative transfer"¹², where downstream performance can be deteriorated therein. Recently, Rong *et al.*¹³ proposed GROVER with delicately-designed, self-supervised pretraining tasks at the node-, edge- and graph-level, respectively. GROVER is pre-trained on c.a. 10M unlabeled molecules, which is then evaluated on 11 benchmark datasets (classification setting: BACE, BBBP, ClinTox, SIDER, Tox21, ToxCast; regression setting: ESOL, FreeSolv, Lipop, QM7, QM8) and achieves SOTA performance in all datasets. The abstracted model architecture of GROVER is depicted in Figure 2. The input node and edge embeddings are first learned via message passing³⁷, which are then passed to the node-view GTransformer and edge-view GTransformer to output the node and edge embeddings from the two views, respectively. With some READOUT function, the final embeddings can be used for node-level, edge-level or graph-level prediction tasks. For downstream tasks, following the practice in Chemprop⁸, GROVER extracts 200 global molecular features using RDKit⁴⁸, which are concatenated with the learned embedding vector, i.e., output of the READOUT function, and then passes through a linear layer, i.e., a task head, for molecular property prediction.

Notably, GROVER has two configurations: GROVER_{base} and GROVER_{large}, corresponding to c.a. 48M and c.a. 100M model parameters, respectively. With c.a. 10M molecules for pretraining, GROVER demands very intensive computational resources. As stated in the paper¹³, GROVER_{base} costs 2.5

days, and GROVER_{large} costs 4 days on 250 NVIDIA V100 GPUs for pretraining. Due to the large number of experiments to be conducted in this study, we only evaluated the pretrained GROVER_{base}. Besides the backbone (weights frozen), there are still one READOUT layer and two 2-layer MLPs, resulting in c.a. 5.2M parameters to fit during finetuning. To examine the actual power of GROVER and the effect of additional RDKit features, we further distinguished GROVER (without RDKit features) and GROVER_RDKit.

2.3 Assembled datasets

To comprehensively evaluate molecular representations and model architectures, the following datasets are assembled.

2.3.1 Opioids with reduced overdose effects

Opioid overdose is a leading cause of injury-related death in the United States⁴⁹. There is an increasing interest in developing opioid analgesics with reduced overdose effects⁵⁰. As pointed out by a large-scale observational study⁵¹, reduced overdose effects can potentially be addressed from the pharmacokinetic (PK) perspective and pharmacodynamic (PD) perspective, which correspond to 1) decreasing overdose events by avoiding excessive amount of opioids in the action site and 2) alleviating overdose outcome by avoiding off-target effects, respectively. The PK-related targets include multi-drug resistance protein 1 (MDR1), cytochrome P450 2D6 (CYP2D6), and CYP3A4 whereas the PD-related targets include μ opioid receptor (MOR), δ opioid receptor (DOR) and κ opioid receptor (KOR). More details are in Section 3.1.

2.3.2 Descriptors datasets with varying sizes

Usually, the property of interest for prediction is the binding activity. However, activity can be innately hard to predict due to the complicated interaction mechanisms¹⁷. Moreover, the datasets are usually limited in size. To evade these constraints by activity, we assembled the descriptor datasets to further interrogate molecular representation learning with regard to predicting simple PhysChem descriptors, namely MolWt and

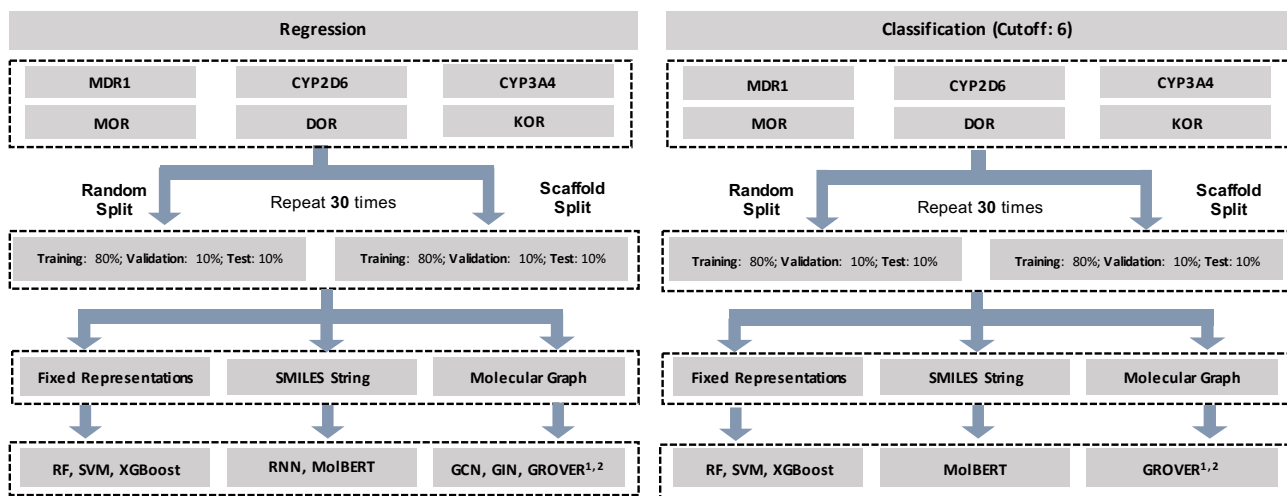


Figure 4. Experiment Scheme in the Opioids-related Datasets. (GROVER^{1,2}: GROVER, GROVER_RDKit)

NumAtoms. Specifically, we assembled datasets with varying sizes (100, 200, ..., 80K, 100K) by randomly sampling from ZINC250K⁵². Details on the datasets are in Section 3.1.

2.4 Study rationale and experiment design

2.4.1 How useful are the learned representations?

The first major question that our study aims to answer is: how useful are the learned representations for molecular property prediction? Previously, although deep neural networks have been reported to outperform traditional machine learning models, such as RF and SVM on ECFP6 in a large-scale activity prediction study⁷, Robinson *et al.*¹⁷ have re-analyzed the results and found that SVM is still competitive with the neural network models. Indeed, whether the learned representations can supersede fixed molecular representations still needs further investigation. To this end, we selected several representative models for molecular property prediction after an extensive literature review⁵. In total, we evaluated traditional machine learning models (RF, SVM and XGBoost), regular neural network models (RNN, GCN and GIN) and pretrained neural network models (MolBERT, GROVER and GROVER_RDKit). The experiment scheme on the MoleculeNet benchmark datasets is in Figure 3. We also evaluated the models using the opioids-related datasets, other activity datasets and descriptor datasets (Figures 4 & 5). In total, we trained 62,820 models.

2.4.2 Are the models properly evaluated?

In MoleculeNet¹⁶, each benchmark dataset comes with a recommended evaluation metric, which is widely adopted by subsequent studies. Specifically, for classification datasets, area under the receiver operating characteristic curve (AUROC) is mostly used; whereas for regression datasets, the most common metric is root mean square error (RMSE). However, these recommended metrics can be problematic. As opined by Robinson *et al.*¹⁷, AUROC for the classification task may be of little relevance in real-world drug discovery applications,

such as virtual screening. In the case of imbalanced datasets, which is often the case in reality where only a small portion of test molecules are actives, AUROC can be biased⁵³. In fact, AUROC can be seen as the expected true positive rate averaged over all classification thresholds (false positive rates). Thus, if two ROC curves cross, even if one curve has higher AUROC, it may perform much worse (lower true positive rate) under certain thresholds of interest. An alternative is area under the precision-recall curve (AUPRC)^{17,53}, which only focuses on the minor class, often the actives.

Here, we further argue that the evaluation metric should be contingent on the question of interest during drug discovery. For instance, one popular sub-task involved in virtual screening is target fishing⁵⁴, which is to identify all possible targets that a molecule can bind to. According to Hu *et al.*⁵⁵, an active PubChem compound can interact with c.a. 2.5 targets and consequently, off-target effects can be pervasive and may lead to undesired adverse drug reactions. Thus, one research area is to identify potential targets for a molecule during early stage⁵⁶. In this scenario, the question is not just about predicting whether a molecule can bind to a specific target. Instead, we would care more about questions like: 1) given a set of predicted drug targets k , what is the fraction of correct predictions among the predicted positives, i.e., *recall@k*; 2) given a set of predicted drug targets k , what is the fraction of correct predictions among the annotated positives, i.e., *precision@k*. Even in the single-target virtual screening scenario, we may care more about the *precision*, which is the positive predictive value (PPV), inasmuch it is imperative to ensure that there is a sufficient amount of true positives out of the predicted positives. On the contrary, if the goal is to exclude molecules inactive against certain targets which are related to adverse reactions, the negative predictive value (NPV) is of more interest. Thus, for each experiment, we evaluated a set of metrics (Figures 3 & 4 & 5). More details on the evaluation metrics are in Section 3.2.

In addition to the evaluation metrics, another crucial but often missing part in previous studies is the statistical test, despite that the benchmark datasets are small-sized^{17,18,57}. Most often, when a new model is developed, some arbitrary split or 3/10-fold splits are applied to calculate the mean of some metric for rudimentary comparison. The reality is, however, due to lack of rigorous statistical tests, such result is insufficient to justify whether there is a true improvement.

Besides, the task settings may also affect the evaluation. Usually, after collecting activity data, i.e., pIC50 values, a cut-off value like 5 or 6 is used to dissect the collected molecules into actives and inactives. Nevertheless, how the classification with an arbitrary cutoff value affects the final prediction compared to directly regressing the pIC50 values hasn't been compared yet. To study the influence of task settings, we conducted experiments under both classification and regression settings for the opioids-related datasets (Figure 4).

2.4.3 What does chemical space generalization mean?

In the representation learning for molecular property prediction, the ultimate goal is to build models that can generalize from seen molecules to unseen ones. To mimic chronological split in the real-world setting, MoleculeNet recommends scaffold split⁵⁸ as a proxy which ensures that molecules in test sets are equipped with unseen scaffolds during training, posing a more challenging prediction task. In the literature, most papers adopt the scaffold-split practice and claim chemical space generalization capability when evaluation metrics are improved. The assumption, notably, is that chemical space generalization is approximated as generalizing between different scaffolds, which further assumes each scaffold is associated with specific properties, for instance, similar activity. Nevertheless, one scaffold may not necessarily map to a narrow range of property values. In this case, the use of scaffold split does not suffice to guarantee chemical space generalization. Moreover, it leads to certain ambiguity.

Formally, the chemical space is defined as the set of all possible organic molecules, in particular, the biologically relevant molecules⁵⁹. In the chemical space, usually there are some structural constellations, which is populated by molecules with specific properties and can be identified using scaffold-based analysis⁶⁰. Since the constellations have diverse scaffolds, two molecules with different scaffolds can have disparate properties, which is termed as the "scaffold cliff"⁶⁰. Using the widely-adopted scaffold split, we argue that it actually addresses the "scaffold cliff" and the model is essentially doing inter-scaffold generalization. Meanwhile, another challenge in drug discovery is the "activity cliffs" (AC), where a tiny structural change causes a drastic activity change between a pair of molecules with similar structures, usually with the same scaffold⁶¹. On the contrary to inter-scaffold generalization, it is the intra-scaffold generalization needed in the case of activity cliffs. Unfortunately, while activity cliffs are prevalent and have been discussed in computational and medicinal chemistry for nearly three decades⁶¹, it has not been emphasized in most molecular property prediction papers. In

this study, we adopted both scaffold split and random split to check inter-scaffold generalization capability (Figures 3 & 4 & 5). Furthermore, to check intra-scaffold generalization, we filtered out molecules with scaffolds observed with the AC issue, denoted as the AC molecules (see Section 4.1.2), and then calculated prediction performance on the AC and non-AC molecules (see Section 4.3.2), respectively.

3 Methods

3.1 Datasets assembly

3.1.1 MoleculeNet benchmark datasets

In 2018, a suite of benchmark datasets from MoleculeNet for molecular property prediction was proposed by Wu et al¹⁶, which have been widely used to develop novel molecular representation learning models. Among them, we selected three classification datasets (BACE, BBBP, HIV) and three regression datasets (ESOL, FreeSolv, Lipop), which are used in MolBERT¹¹ and GROVER¹³ (except for HIV) as well as a recent comparison study Jiang et al⁴². Note that these datasets are for single-task purpose and were downloaded from MolMapNet¹⁹, which has a more updated version. Each dataset and its task type, number of molecules, maximum length and number of scaffolds are summarized in Table 3. Since MolBERT needs to pad the input SMILES strings to the maximum length, we only retained molecules with length no longer than 400, which is applied to all models for fair comparison. As shown in Table 3, all selected benchmark datasets have maximum length less than 400 except for HIV, where c.a. 0.01% molecules were removed.

Dataset	Task	#Mol.	Max. Len.	#Scaff.
BACE	CLS	1,513	198	737
BBBP	CLS	2,039	400	1,101
HIV	CLS	41,127	580	19,085
ESOL	REG	1,128	98	268
FreeSolv	REG	642	82	62
Lipop	REG	4,200	267	2,443

Table 3. Summary of the MoleculeNet Benchmark Datasets.

As for dataset splitting, there are several options, such as random split, scaffold split, stratified split and time split¹⁶. Each method has its own purpose. For example, time split makes the model trained on older data points and tested on newer molecules, which mimics the real-world scenario where models are built on existing data points and are used to predict properties of newly synthesized molecules¹⁶. The most widely adopted method in the literature is scaffold split, which addresses the inter-scaffold generalization (see Section 2.4.3). However, actual splits can vary across studies. For instance, for the regression datasets, MolBERT¹¹ used the random splits provided in MolMapNet¹⁹ while GROVER adopted scaffold split. For the classification datasets, both MolBERT and GROVER adopted scaffold split, although the seeds are not provided and thus the splits may not be identical.

In this study, we adopted both scaffold and random split, following a 80:10:10 ratio for training/validation/test sets (Figures 3 & 4 & 5). Additionally, to ensure sufficient statistical rigor, we repeated the dataset split procedure 30 times with 30 different seeds (0, 1, 2, \dots , 29) using GROVER’s implementation for dataset split, which were saved and kept the same for all experiments to ensure fair comparison.

3.1.2 Opioids-related datasets

To check the usefulness of the representation learning models for molecular property prediction, we also assembled a suite of opioids-related datasets (see Section 2.3.1). Specifically, we collected the binding affinity for the following pharmacological components^{51,62}: MDR1 (ChEMBL ID: 4302), CYP2D6 (ChEMBL ID: 289), CYP3A4 (ChEMBL ID: 340), MOR (ChEMBL ID: 233), DOR (ChEMBL ID: 236) and KOR (ChEMBL ID: 237). The binding affinity data is retrieved from ChEMBL27²² using *in vitro* potency measures, namely, IC50, EC50, Ki and Kd. Assay type is set as "Binding", standard relationship is set as "=" with the standard unit as "nM" and the organism as "Homo Sapiens". The raw binding affinity data is further converted into the negative log 10 scale, which is denoted as pIC50. Lastly, we cleaned the datasets by removing contradictory entries and duplicates.

Notably, IC50/EC50/Ki/Kd are often heteroscedastic⁶³. Consequently, measurement errors are not equally distributed throughout the range of activity and, therefore, regression of the raw pIC50 values may not be favorable⁶³. Thus, one common practice is to convert direct regression into a binary classification task. For the active vs. inactive threshold, 1 μ M (pIC50 at 6) is usually used as the default cutoff. Here, we also adopted this practice (Figure 4).

Dataset	Task	#Mol.	Max. Len.	#Scaff.
MDR1	CLS-REG	1,438	252	602
CYP2D6	CLS-REG	2,293	217	1,330
CYP3A4	CLS-REG	3,671	244	2,022
MOR	CLS-REG	3,553	373	1,623
DOR	CLS-REG	3,223	373	1,531
KOR	CLS-REG	3,326	373	1,660

Table 4. Summary of the Opioids-related Datasets.

The task type, together with number of molecules, maximum length and number of scaffolds, are summarized in Table 4. Since all datasets have a maximum length less than 400, the collected molecules are 100% retained. For the opioids-related datasets, we also applied both scaffold and random split (Figure 4), each of which was repeated 30 times with 30 different seeds (0, 1, 2, \dots , 29) in GROVER’s implementation for dataset split. The data splits were also saved and kept the same in all subsequent experiments.

3.1.3 Descriptor datasets

To further interrogate the representation learning models’ predictive power, we formed the descriptor datasets with sim-

ple molecular descriptors as labels, namely MolWt and NumAtoms. The descriptor datasets have varying sizes from 100 to 100,000, which were randomly sampled from ZINC250k⁵² and calculated by functions in RDKit⁴⁸. The experimental scheme on the descriptor datasets is in Figure 5b, where we also adopted both scaffold and random split, following a 80:10:10 ratio for training/validation/test sets. Again, to ensure sufficient statistical rigor, we repeated the dataset split procedure 30 times with 30 different seeds (0, 1, 2, \dots , 29) using GROVER’s implementation for dataset split, which were saved and kept the same in all experiments.

3.1.4 Other activity datasets

To fully evaluate the models’ predictive performance, we also assembled two other sets of activity datasets from literature. The first set is proposed by Cortés-Ciriano et al²³, which contain activity data for 24 drug targets. The experiment scheme on these activity datasets 1 is depicted in Figure 5a, where we adopted both scaffold and random split, following a 80:10:10 ratio for training/validation/test sets. Again, to ensure sufficient statistical rigor, we repeated the dataset split procedure 30 times with 30 different seeds (0, 1, 2, \dots , 29) using GROVER’s implementation for dataset split, which were saved and kept the same to ensure fair comparison. The second set is proposed in MoleculeACE by Tilborg et al²⁴, which contains activity data for 30 drug targets. The activity datasets by Tilborg et al highlights the activity-cliffs issue and provides a fixed training-test split, based on which we tested traditional machine learning models on fixed molecular representations.

3.2 Evaluation metrics

In Section 2.4.2, we discussed why the recommended metric may not be proper for model evaluation. Details on other basic metrics are illustrated as follows. Note there are more sophisticated virtual screening metrics in early discovery, like area under the accumulative curve (AUAC), Boltzmann-Enhanced Discrimination of ROC (BEDROC), enrichment factor (EF) and robust initial enhancement (RIE), among others⁶⁴.

3.2.1 Classification metrics

In a binary classification task setting, a probability for each molecule as the positive (or active) class is usually assigned. When the estimated probability is greater than a threshold (a value between 0 and 1), the molecule is classified as positive (or active), otherwise negative (or inactive). In total, there are four possible outcomes: true positive (TP), false positive (FP), true negative (TN) and false negative (FN). Based on the TP and FP rates across different probability thresholds, the receiver operating characteristic curve can be plotted with the area under the ROC curve as AUROC. Similarly, based on precision and recall, the precision-recall curve can be plotted and AUPRC is calculated likewise. AUROC usually ranges from 0.5 and 1, with 0.5 for random classification and 1 for perfect classification; in the case of a classifier worse than random guessing, AUROC can be lower than 0.5. Compared

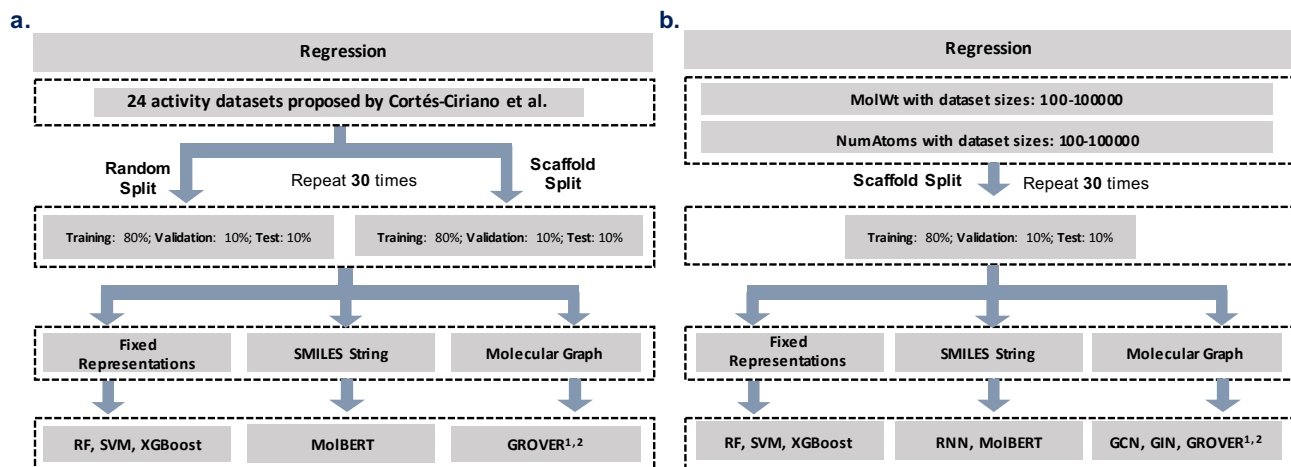


Figure 5. Experiment Scheme in **a.** Bender Activity and **b.** Descriptor Datasets. (GROVER^{1,2}: GROVER, GROVER_RDKit)

to accuracy, AUROC is more robust in the case of imbalanced datasets¹⁷. Nonetheless, by assuming equal importance of positive and negative classes, AUROC may suffer from imbalanced datasets, especially when the minor class is more of interest¹⁷. Thus, AUPRC is proposed as an alternative when datasets are imbalanced⁵³, with the baseline value as the proportion of the minor class.

$$PPV = \frac{TP}{TP + FP} \quad (1)$$

$$NPV = \frac{TN}{TN + FN} \quad (2)$$

Despite the usefulness of AUROC and AUPRC, these "collective" metrics may not be directly pertinent to virtual screening¹⁷, a common application for molecular property prediction⁵. In fact, the primary goal of early drug discovery is to rank molecules based on the predicted activity so as to avoid the intractable number of false positives or false negatives to be filtered out experimentally⁶⁵. Given a set of predicted actives or inactives, depending on the screening goal, we argue that positive predictive value (PPV; Equation 1) and negative predictive value (NPV; Equation 2) are more relevant to virtual screening and drug design, as discussed in Section 2.4.2. Notably, unlike AUROC and AUPRC which are averaged across different probability thresholds, a decision threshold is determined first before deriving the TP, FN, TN and FP, based on which PPV and NPV are calculated. When the datasets are balanced, the decision threshold for positive vs. negative is set as 0.5. However, for imbalanced datasets, the threshold needs to be adjusted. Here, we used Youden's J statistic⁶⁶, the distance between the ROC curve and the random chance line, to adjust threshold which maximizes the J statistic.

3.2.2 Regression metrics

For the regression task, RMSE (Equation 3) and MAE (Equation 4) are the recommended metrics, which indicate how apart the predicted values are from the labels: a lower value stands for a better model fit. MAE is a natural measure of average error whereas RMSE gives more weight to large errors and is more sensitive to the outliers. In addition, two other metrics can also measure the regression performance^{8,16,67}, namely, Pearson_R and R2, which are scale independent.

$$RMSE = \sqrt{\frac{1}{N} \sum_{i=1}^N (y_i - \hat{y}_i)^2} \quad (3)$$

$$MAE = \frac{1}{N} \sum_{i=1}^N |y_i - \hat{y}_i| \quad (4)$$

$$Pearson_R = \frac{\sum_{i=1}^N (y_i - \bar{y}_{obs})(\hat{y}_i - \bar{y}_{pred})}{\sqrt{\sum_{i=1}^N (y_i - \bar{y}_{obs})^2 \sum_{i=1}^N (\hat{y}_i - \bar{y}_{pred})^2}} \quad (5)$$

$$R2 = 1 - \frac{\sum_{i=1}^N (y_i - \hat{y}_i)^2}{\sum_{i=1}^N (y_i - \bar{y}_{obs})^2} \quad (6)$$

Pearson_R is an intuitive measure of the linear correlation between the predicted values and labels⁶⁸, which is the ratio between the covariance of two variables and the product of their standard deviations (Equation 5), ranging from -1 to 1. An absolute value of 1 indicates a perfect linear relationship between the predicted values and labels. Notably, some studies used Pearson_R⁶⁷ while other papers used the square of Pearson_R^{16,19}, i.e., Pearson_R2, which always ranges from 0 to 1. On the other hand, R2, also known as the coefficient of determination, is not based on correlation. Instead, R2 calculates the proportion of the variance in the predicted values

Statistical Test	Alias	Parametric	Normality	Equal Variance	Equal Size
Paired t test	Dependent t test	✓	✓	✓	✓
Unpaired t test	Independent or Welch’s t test	✓	✓	×	×
Wilcoxon signed-rank test	-	×	×	✓	✓
Wilcoxon rank-sum test	Mann-Whitney U test	×	×	×	×

Table 5. Summary of the Statistical Tests.

that can be explained by the labels (Equation 6). Usually, R^2 ranges from 0 to 1. A higher R^2 corresponds to a better model fit. The best scenario is that the predicted values exactly match the observed values and R^2 would be 1. On the contrary, the baseline case is that the model always predicts \bar{y}_{obs} and R^2 would be 0. Worse still, when models have poorer predictions than the baseline, R^2 can even be negative. Presumably due to naming similarity, R^2 and Pearson_ R^2 can sometimes be messed with each other. In this study, we included both Pearson_ R and R^2 , which are calculated with the `scipy` package and the `scikit-learn` package, respectively.

3.3 Model training

The hyperparameters of traditional machine learning models were determined by using grid search around the default values or reported values in the literature and selecting the best performance combination on the validation set. For regular neural network models, we set the hyperparameters such that the models in comparison have similar number of parameters. Specifically, we followed Chemprop⁸ and set the number of trees as 500 for RF. For SVM, we used the linear support vector regressor or classifier whereas for XGBoost, we used the gradient boosting regressor or classifier. The remaining hyperparameters are set as default. For RNN, we adopted the GRU variant and set the hidden size as 512, followed by 3 fully connected layers. For GCN and GIN, the embedding dimension is 300, followed by 5 convolutional layers and the dimension for hidden vectors is set as 512¹⁴. For MolBERT and GROVER, we adopted the optimal hyperparameters reported in the original papers and also trained them for 100 epochs^{11,13}. All experiments with the deep learning models were run on a single NVIDIA V100 GPU for 100 epochs. The validation loss is used to select the best model during training for later test purpose. The batch size is set as 32. However, for the HIV dataset, MolBERT takes around 3 hours to complete a 100-epochs training in each split when the batch size is 32. Since GROVER takes even more time, we set the batch size as 256 when applying GROVER on HIV, which still takes around 5 hours to complete a 100-epoch training. To ensure fair comparison, we saved all raw predictions, based on which prediction performance were calculated using the same codes.

3.4 Statistical analyses

To examine if the prediction performance is significantly improved by the representation learning models, we conducted statistical analyses on the prediction performance. Usually, two major categories of analyses can be applied: paramet-

ric and non-parametric tests⁶⁹ (Table 5). Among them, the parametric t tests examine whether two groups have equal means, which can be further categorized into paired t test and unpaired t test. For the paired t test, the null hypothesis is that the means of two populations are equal, underlying by the equal-variance assumption. When two samples have unequal variances and/or unequal sample sizes, the unpaired or independent t test, a.k.a. Welch’s t test, should be used. Notably, the paired and independent t tests are parametric tests with the normality assumption. When the sample size is large, the t tests can still be robust to moderate violations of the normality assumption. Nonetheless, if the normal assumption is violated and the sample size is small, non-parametric tests should be used instead, namely, Wilcoxon signed-rank test and Wilcoxon rank-sum test. Wilcoxon signed-rank test uses the signed rank to compare the medians of two populations, which is a non-parametric version of the paired t test. Wilcoxon rank-sum test, a.k.a. Mann-Whitney U test, also compares the medians but is robust to the violations of homoscedasticity. Neither Wilcoxon signed-rank test nor Wilcoxon rank-sum test requires the normality distribution. However, when the data are normally distributed, the non-parametric tests may lead to less statistical power, which corresponds to a higher probability of making the type II error (false negative)^{17,69}.

In this study, since the distribution of each metric is not normal and variance is non-equal (Sup. Fig 13-15), we adopted the non-parametric Mann Whitney U test to calculate the pairwise significance. The statistical significance is set as the two-sided p value less than 0.05.

4 Results

4.1 On the datasets

4.1.1 Label and structure profiling

To have a clear grasp on the datasets, we conducted label profiling for the MoleculeNet benchmark datasets and the opioids-related datasets. As shown in Figure 6a, BACE is balanced with a positive rate of 45.7%, whereas BBBP is imbalanced towards the positives (76.5%) and HIV has much less positive instances (3.5%). The labels of ESOL, FreeSolv and Lipop all exhibit left-skewed distribution, especially for FreeSolv. On the other hand, the pIC50 distribution for the opioids-related datasets is right-skewed (Figure 6b), presumably because most screened molecules exhibited low activity to the targets. To construct the opioids-related datasets in the classification setting, we applied a cutoff at 6 on the raw pIC50 values to convert them into binary values, namely ac-

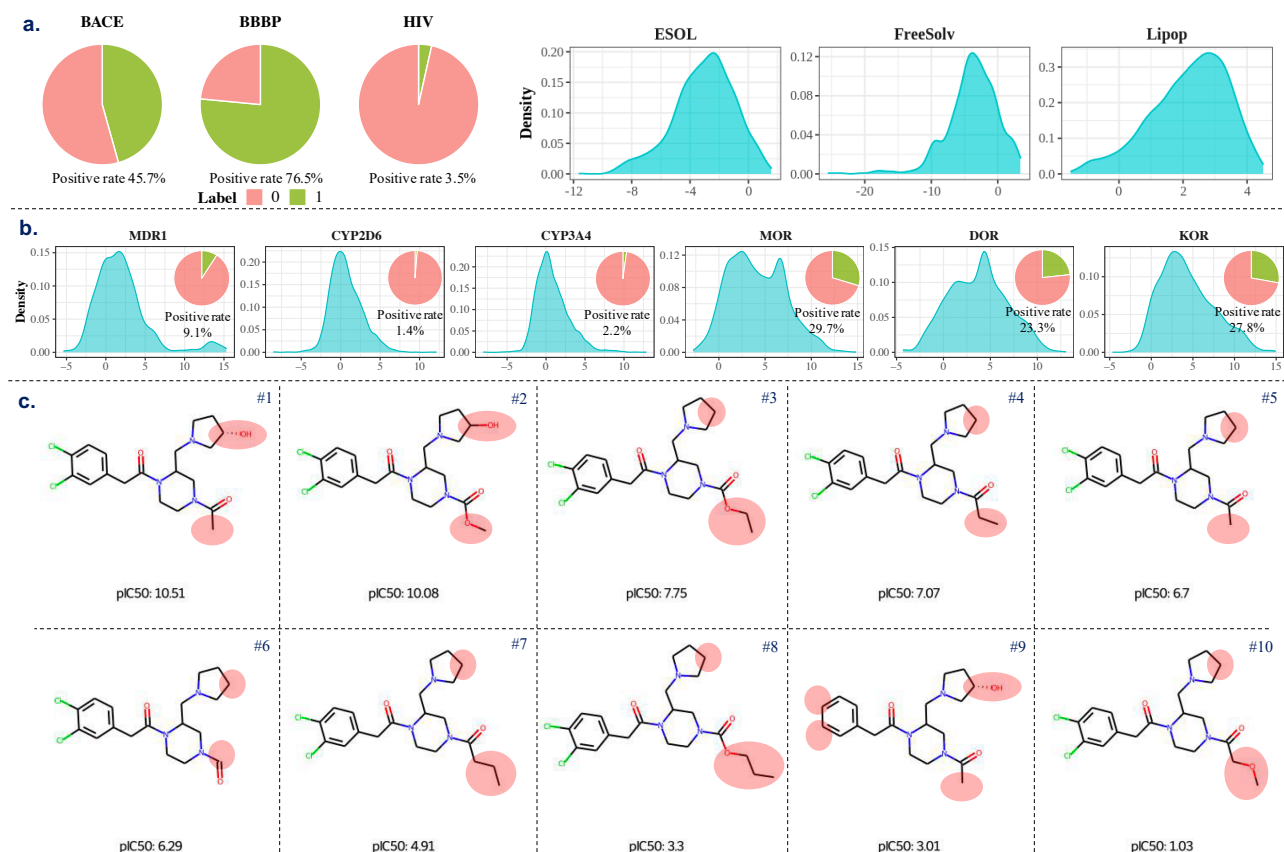


Figure 6. Datasets Profiling for the Benchmark and Opioids-related Datasets. **a.** Label distribution for the selected MoleculeNet benchmark datasets. **b.** Label distribution in the opioids-related datasets. **c.** Activity-cliffs showcase on a series of molecules with the KOR Top 14 scaffold (Sup. Figure 10).

tive and inactive, abiding by the rule that pIC50 less than 6 inactive otherwise active. As shown in Figure 6b, the resultant datasets are all imbalanced. For MOR, DOR and KOR, the positive rates are 29.7%, 23.3% and 27.8%, respectively. For MDR1, CYP2D6, CYP3A4, the positive rates are even lowered to 9.1%, 1.4% and 2.2%.

To quantify the difference of label distributions, we calculated the Kolmogorov D statistic⁷⁰ among the training, validation and test sets (Sup. Figure 1a). When using scaffold split, the D statistic is more dispersed with a higher median than that when using random split, suggesting that scaffold split leads to larger gaps in the label distributions in addition to separating molecules by the scaffolds, which, to some extent, manifests that molecules with same scaffolds tend to have similar properties. Random split, on the other hand, results in a more compact distribution of the D statistic with a lower median, indicating that training and test sets are more likely to have molecules with close labels. To quantify the structural similarity among the training, validation and test sets, we also calculated the Tanimoto similarity⁷¹, shown in Sup. Figure 1b. Likewise, Tanimoto similarity exhibits more compact distribution under random split, the median of which are also higher, showing that training and test molecules are more structurally

similar compared to those under scaffold split.

We also calculated the percentage of top fragments, i.e., heterocycles and functional groups, for both MoleculeNet benchmark and opioids-related datasets, which are summarized in Sup. Figures 2 & 3. The top heterocycles vary across different datasets, which also manifest their unique pharmacological properties. For instance, the top heterocycle is piperidine for MOR, DOR and KOR (Sup. Figure 3a), which is commonly seen in opioid analgesics⁷². For the functional groups, all datasets share top functional groups such as benzenes and amines, which are common components to facilitate the interaction with drug targets, typically proteins with abundant amino acid residues, via forming hydrogen bonds or π - π stacking interactions⁷³. Other structural traits, such as number of rotatable bonds and the number of rings, are summarized in Sup. Figure 4.

For the other two activity datasets and descriptor datasets, the label distributions are summarized in Sup. Figure 11.

4.1.2 Activity cliffs in opioids-related datasets

For molecular property prediction, the essential goal is to achieve chemical space generalization, which, ideally, encompasses both inter-scaffold and intra-scaffold generalization

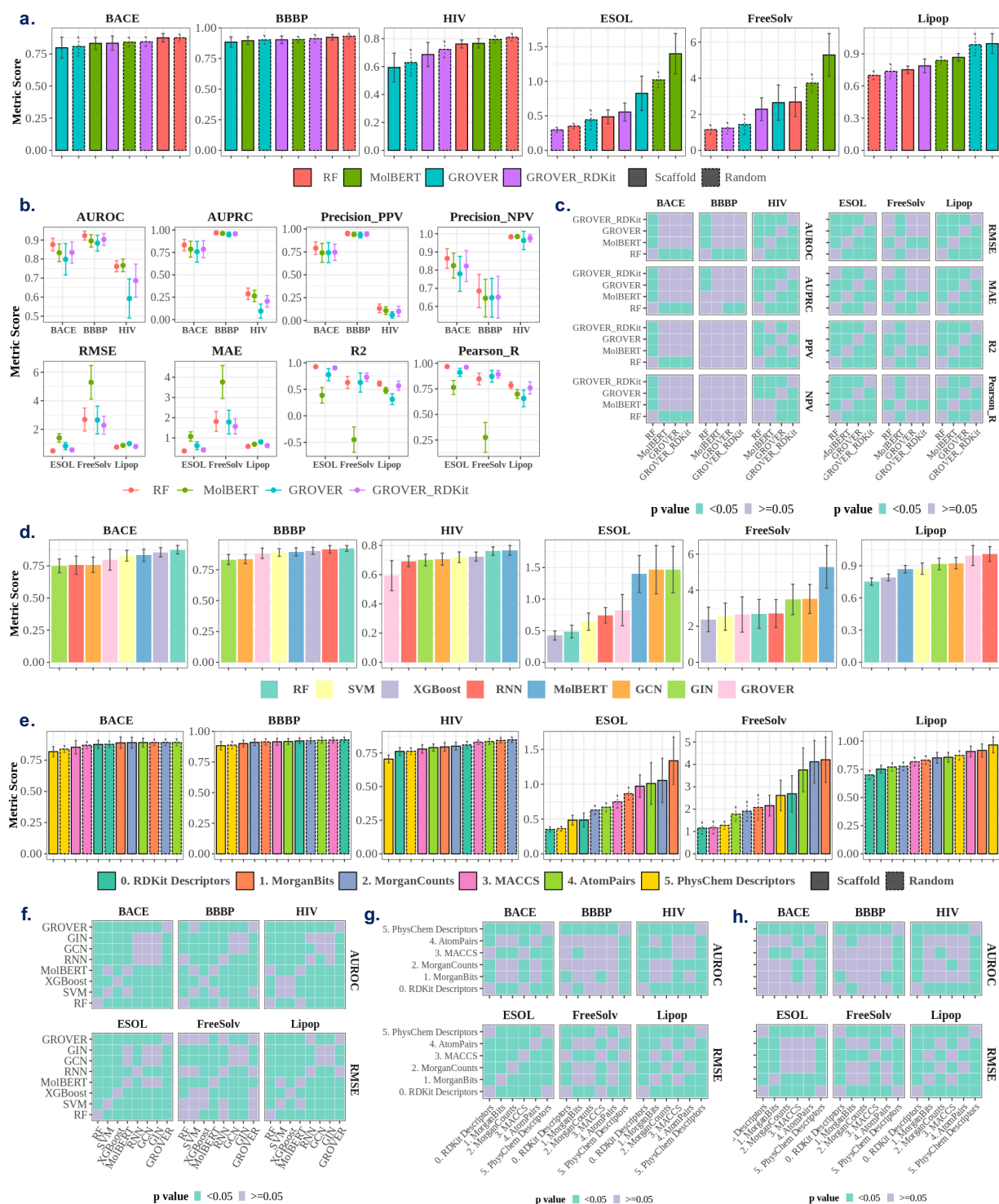


Figure 7. Performance in MoleculeNet Benchmark Datasets (errorbar: standard deviation). **a.** Performance of RF on RDKit2D descriptors, MolBERT, GROVER and GROVER_RDKit using recommended metrics. **b.** Performance of RF on RDKit2D descriptors, MolBERT, GROVER and GROVER_RDKit under scaffold split. **c.** Mann-Whitney U significance for plot **b**. **d.** Performance of RF, SVM & XGBoost on RDKit2D descriptors, RNN & MolBERT and GCN, GIN & GROVER under scaffold split. **e.** Performance of RF on fixed representations. **f.** Mann-Whitney U significance for plot **d**. **g.** Mann-Whitney U significance for plot **e** under random split. **h.** Mann-Whitney U significance for plot **e** under scaffold split.

(see Section 2.4.3). Scaffold split, which ensures no scaffold overlap among training, validation and test sets, addresses the inter-scaffold challenge and has been widely adopted in the literature. However, the intra-scaffold generalization, especially in the case of activity cliffs, has not been well addressed yet. Thus, we proposed to evaluate the intra-scaffold generalizability using the opioids-related datasets.

For each target, we visualized the top 30 scaffolds along with its pIC50 distribution (Sup. Figures 5-10). To showcase activity cliffs where analogs exhibit drastic difference in potency, we illustrated with the KOR Top 14 scaffold (Sup. Figure 10). As shown in Figure 6c, the replacement of the two hydrogen atoms with the chlorine atoms at the phenyl ring from molecule #9 to molecule #1 results in a drastic activity increase by 7 orders of magnitude, which, presumably, is because the chlorine atoms help the ligand better occupy the hydrophobic space in the binding pocket, an important contributor for binding. When comparing molecule #1 to molecule #5, the hydroxyl group at the pyrrolidine ring increases the potency by 4 orders of magnitude, which also indicates that a potential H-bond interaction with the receptor is crucial for binding. Meanwhile, although shortening the acetyl group to the aldehyde group poses a minor reduction in activity when contrasting molecule #5 to molecule #6, longer side chains (molecules #7 & #8) can undermine activity, which suggests limited space around the binding site.

Dataset	#AC. Scaff. (%)	#Mol. AC. Scaff. (%)
MDR1	62 (10.2)	594 (41.3)
CYP2D6	124 (9.3)	710 (31.0)
CYP3A4	146 (7.2)	926 (25.2)
MOR	213 (13.1)	1,627 (46.1)
DOR	178 (11.6)	1,342 (41.6)
KOR	218 (13.1)	1,502 (45.2)

Table 6. Summary of Activity Cliffs in the Opioids Datasets.

These molecules show that major activity change can happen even with minor structural changes. More formally, we defined the activity cliffs as IC50 values spanning at least two orders of magnitude within one scaffold^{61,74}. Note that one order of magnitude can be also used. The scaffolds observed with activity cliffs are termed as the AC scaffolds and molecules with the AC scaffolds are denoted as the AC molecules. The number (percentage) of AC scaffolds and AC molecules are summarized in Table 6. Notably, although AC scaffolds percentages are around 10%, nearly half molecules are equipped with the AC scaffolds in MDR1, MOR, DOR and KOR, posing a challenge for intra-scaffold generalization.

4.2 On the model evaluation

4.2.1 Does learned representation surpass descriptors?

We first compared prediction performance of RF to pretrained models, which are reported to achieve SOTA performance, namely, MolBERT, GROVER and GROVER_RDKit. Since RDKit2D descriptors are utilized in GROVER_RDKit, we

used it as the fixed representation to RF. Under scaffold split shown in Figure 7a, RF achieves best performance in BACE, BBBP, ESOL, Lipop whereas MolBERT achieves best performance in HIV ($p < 0.05$). In FreeSolv, GROVER and GROVER_RDKit achieves similarly low RMSE with RF whereas MolBERT has the highest RMSE ($p < 0.05$). Similarly, in ESOL and 22 activity datasets by Cortés-Ciriano et al (Figure 10), MolBERT shows the highest RMSE ($p < 0.05$). In Lipop, erbb1 and HERG where dataset size increases to around 4,000, however, MolBERT shows better performance than GROVER, which, again, is still outperformed by RF and GROVER_RDKit ($p < 0.05$). We speculate that when dataset size increases, MolBERT may exhibit more prediction power.

Moreover, by comparing GROVER and GROVER_RDKit, we observed that concatenating RDKit2D descriptors significantly improves GROVER’s performance in all benchmark datasets (Figure 7a) except FreeSolv (dataset size: 642). Similar observation can be made in opioids-related datasets (Figure 8a & Figure 9a), except CYP2D6 at classification setting. Among the 24 activity datasets by Cortés-Ciriano et al, 9 datasets are observed with significantly lower RMSE in GROVER_RDKit compared to GROVER. Thus, concatenating RDKit2D descriptors to the learned representations may be misleading when evaluating the real power of the representation learning models. Due to the non-negligible effect of RDKit2D descriptors, we only included GROVER when comparing major molecular representations, namely RDKit2D descriptors, SMILES strings and molecular graphs (Figures 7d & 8d). Indeed, as supported by most datasets, RDKit2D descriptors show better performance than learned representations by RNN, GCN, GIN and pretrained models using either SMILES strings or molecular graphs.

For RDKit2D descriptors, we also compared different machine learning models (Figures 7d & 8d) and found that RF achieves best performance in BACE, BBBP, HIV, Lipop and all opioids-related datasets whereas XGBoost is best in ESOL and FreeSolv ($p < 0.05$). SVM exhibits worst performance in all opioids-related datasets at regression setting (Figure 8d) and most benchmark datasets (Figure 7d). For SMILES strings, pretrained MolBERT outperforms RNN in BACE, HIV, Lipop and all opioids-related datasets except MDR1. For molecular graphs, we found GCN and GIN achieves similar performance. GROVER outperforms GCN and GIN in BACE, BBBP, ESOL and FreeSolv whereas in HIV, Lipop and the opioids-related datasets (bigger dataset sizes), GROVER shows worse performance. On the contrary to MolBERT, we speculate that when dataset size decreases, GROVER may exhibit more prediction power.

4.2.2 Are the statistical tests necessary?

To demonstrate the necessity of statistical tests, we conducted a simple analysis by comparing RF on RDKit2D descriptors, MolBERT, GROVER using the benchmark datasets, which tries to answer: using the average metric value alone and under scaffold split, the widely-adopted practice, how many 1-fold or 3-fold splits combination out of the 30-fold splits are

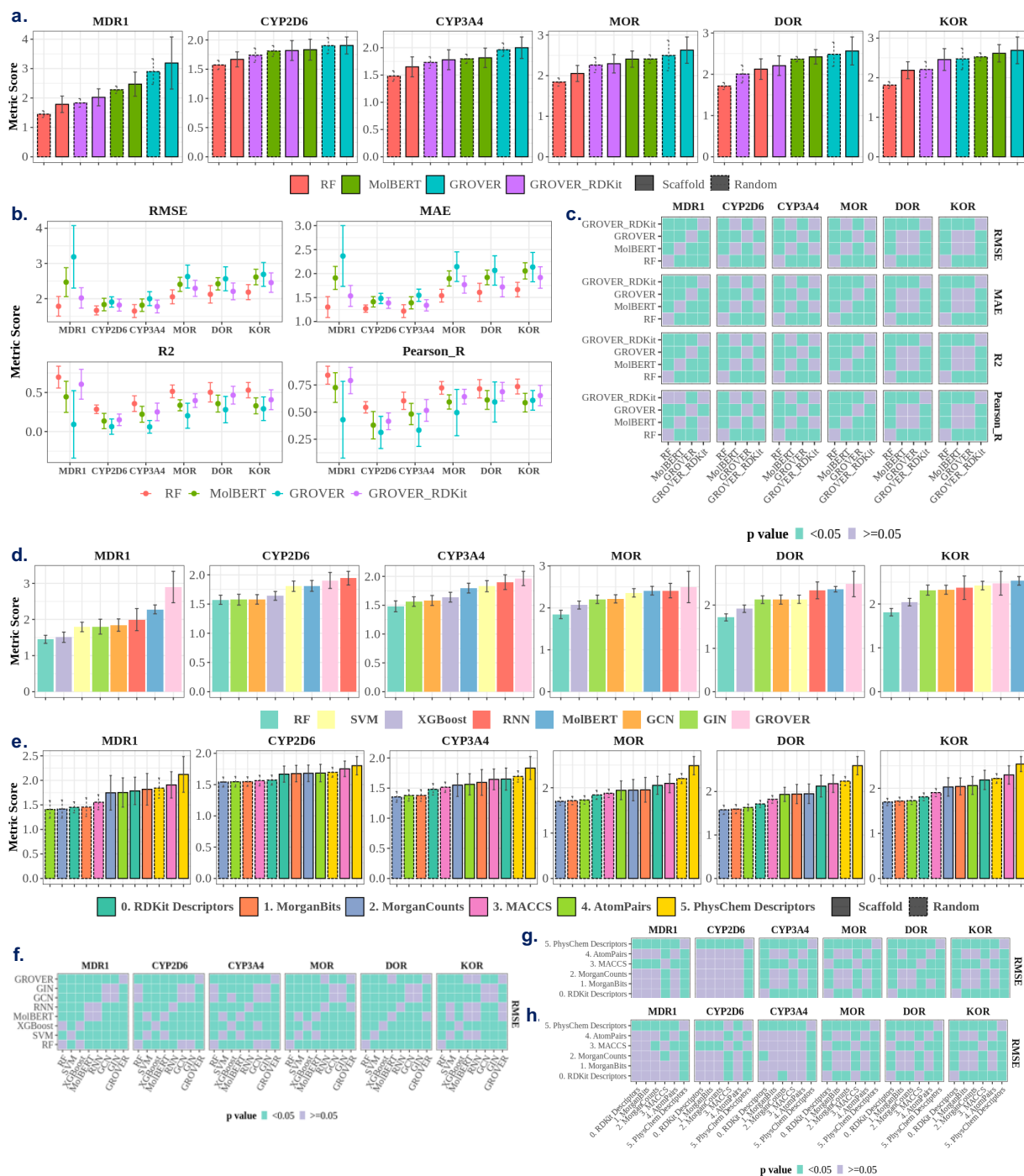


Figure 8. Performance in Opioids-related Datasets at Regression Setting (errorbar: standard deviation). **a.** Performance of RF on RDKit2D descriptors, MolBERT, GROVER and GROVER_RDKit. **b.** Performance of RF on RDKit2D descriptors, MolBERT, GROVER and GROVER_RDKit under scaffold split. **c.** Mann-Whitney U significance for plot **b**. **d.** Performance of RF, SVM & XGBoost on RDKit2D descriptors, RNN & MolBERT and GCN, GIN & GROVER under scaffold split. **e.** Performance of RF on fixed representations. **f.** Mann-Whitney U significance for plot **d**. **g.** Mann-Whitney U significance for plot **e** under random split. **h.** Mann-Whitney U significance for plot **e** under scaffold split.

there for a certain model to be concluded as best-performing?
Note that GROVER_RDKit is removed from this analysis

because concatenation of RDKit descriptors can significantly bias the comparison (see Section 4.2.1).

Model	RANDOM FOREST	MOLBERT	GROVER
BACE	23	6	1
BBBP	20	6	4
HIV	11	18	1
ESOL	30	0	0
FreeSolv	12	0	18
Lipop	30	0	0

Table 7. Number of 1-Fold Splits where a Model Achieves the Best Performance under Scaffold Split.

For RF, MolBERT and GROVER (denoted as GROVER¹), we first calculated the number of single test fold where a model achieves best performance using the recommended metrics (Table 7). In BACE, BBBP, ESOL and Lipop, RF dominates across 23, 20, 30 and 30 splits, respectively, which is consistent with the finding in Section 4.2.1, that is, RF is best performing. Still, there are other splits where MolBERT or GROVER achieves the highest AUROC in the classification datasets, which means there is a chance to wrongly conclude the representation learning models as best-performing. Moreover, to emulate the common 3-fold splits practice, we also calculated the number of 3-fold splits where a specific model predicts best based on the average of recommended metrics. Table 8 shows that there are quite some combinations where a model can be mistaken as best performing. For the analysis with other metrics, readers can refer to Sup. Tables 1 & 2.

Model	RANDOM FOREST	MOLBERT	GROVER
BACE	3,644	23	393
BBBP	3,189	408	463
HIV	1,404	2,635	21
ESOL	4,060	0	0
FreeSolv	1,450	0	2,610
Lipop	4,060	0	0

Table 8. Number of 3-Fold Splits Combinations where a Model Achieves the Best Performance under Scaffold Split.

Thus, without statistical tests, chances are that wrong conclusions can be drawn with regard to whether a new technique truly advances the predictive performance. Moreover, since the benchmark datasets are public, one caveat is that the data splitting might be customized to cater to a specific model.

4.2.3 Which fixed representation is most powerful?

Given the superior performance of RF in most datasets (see Section 4.2.1), we mainly analyzed results by RF on fixed molecular representations, namely RDKit2D descriptors, PhysChem descriptors, MACCS keys, MorganBits fingerprints, MorganCounts fingerprints and AtomPairs fingerprints. Notably for MorganBits, we compared different sizes for radius (2, 3) and numBits (1024, 2048) using the benchmark and opioids-related datasets. Since there is little difference when altering the sizes (Sup. Figure 12), we stuck with

radius 2 and numBits 2048 for the Morgan fingerprints.

Among all fixed representations, PhysChem descriptors show worst performance in most datasets (Figures 7e & 8e & 9d & 10c), presumably due to its limited features. Surprisingly in ESOL and FreeSolv, however, PhysChem descriptors achieves best performance along with RDKit2D descriptors and MACCS keys. In other datasets, RDKit2D descriptors is significantly better than PhysChem descriptors except in A2a (dataset size: 166), ABL1 (dataset size: 536), Dopamine (dataset size: 405), possibly due to overfitting. For MorganBits fingerprints, a widely-used strong baseline, we observed that it outperforms RDKit2D descriptors in HIV whereas in ESOL, FreeSolv and Lipop, it is outperformed by RDKit2D descriptors. However, when the datasets are related to binding, for instance, BACE, the opioids-related datasets and most activity datasets by Cortés-Ciriano et al, MorganBits vectors exhibits significantly better performance. As for MorganBits and MorganCounts fingerprints, there is no significant difference except in ESOL and Lipop, where MorganCounts outperforms MorganBits. For AtomPairs fingerprints, it can show similarly superior performance with MorganBits and MorganCounts. For MACCS keys, despite showing best performance in FreeSolv, it generally shows worse performance than MorganBits, MorganCounts and AtomPairs fingerprints.

4.2.4 Are the recommended metrics appropriate?

In MoleculeNet¹⁶, each benchmark dataset comes with a recommended evaluation metric. However, in real-world drug discovery, the recommended metrics may not be pertinent (see Section 2.4.2). In this section, we compared the model performance using a set of evaluation metrics in addition to the recommended ones. For classification tasks, we calculated AUROC, AUPRC, PPV and NPV (see Section 3.2.1); for regression tasks, we calculated RMSE, MAE, R2 and Pearson_R (see Section 3.2.2). As shown in Figure 7b & c, when using the recommended AUROC, RF achieves higher performance than MolBERT, GROVER and GROVER_RDKit in BBBP ($p < 0.05$). However, if the evaluation metric is PPV or NPV, RF shows similar performance with all the other three models. Another example is that, when evaluated by AUROC, MolBERT achieves significantly higher performance in HIV compared to GROVER_RDKit; but when evaluated by PPV, MolBERT shows similar performance with GROVER_RDKit ($p \geq 0.05$). Thus, different metrics may lead to disparate conclusions and caution is needed, especially for those with similar naming, such as R2 and Pearson_R. In fact, by plotting R2 against Pearson_R, we found Pearson_R can overestimate R2 (Sup. Figure 18a). In some cases, Pearson_R can still be around 0.5 even when R2 drops to nearly zero or negative. As for RMSE vs MAE, RMSE shows greater value than MAE given the same prediction results (Sup. Figure 18b).

As for which metrics are appropriate, we observed that in the opioids-related datasets, AUROC is generally over 0.75 except in CYP2D6 (Figure 9a), whereas most AUPRC drops below 0.75 (Figure 9b). For MolBERT, GROVER and GROVER_RDKit, AUPRC drops to c.a. 0.25 in CYP3A4



Figure 9. Performance in Opioids-related Datasets at Classification Setting (errorbar: standard deviation). **a.** Performance of RF on RDKit2D descriptors, MolBERT, GROVER and GROVER_RDKit. **b.** Performance of RF on RDKit2D descriptors, MolBERT, GROVER and GROVER_RDKit under scaffold split. **c.** Mann-Whitney U significance for plot **b**. **d.** Performance for RF on fixed representations. **e.** Mann-Whitney U significance for plot **d** under random split. **f.** Mann-Whitney U significance for plot **d** under scaffold split. **g.** Percentage of edge-case molecules in test sets. **h.** AUROC of RF on MorganBits after edge-case removal. **i.** Prediction errors of RF on MorganBits for all molecules at regression setting under scaffold split. **j.** Predicted probability from RF on MorganBits for edge-case molecules under scaffold split with various cutoff values.

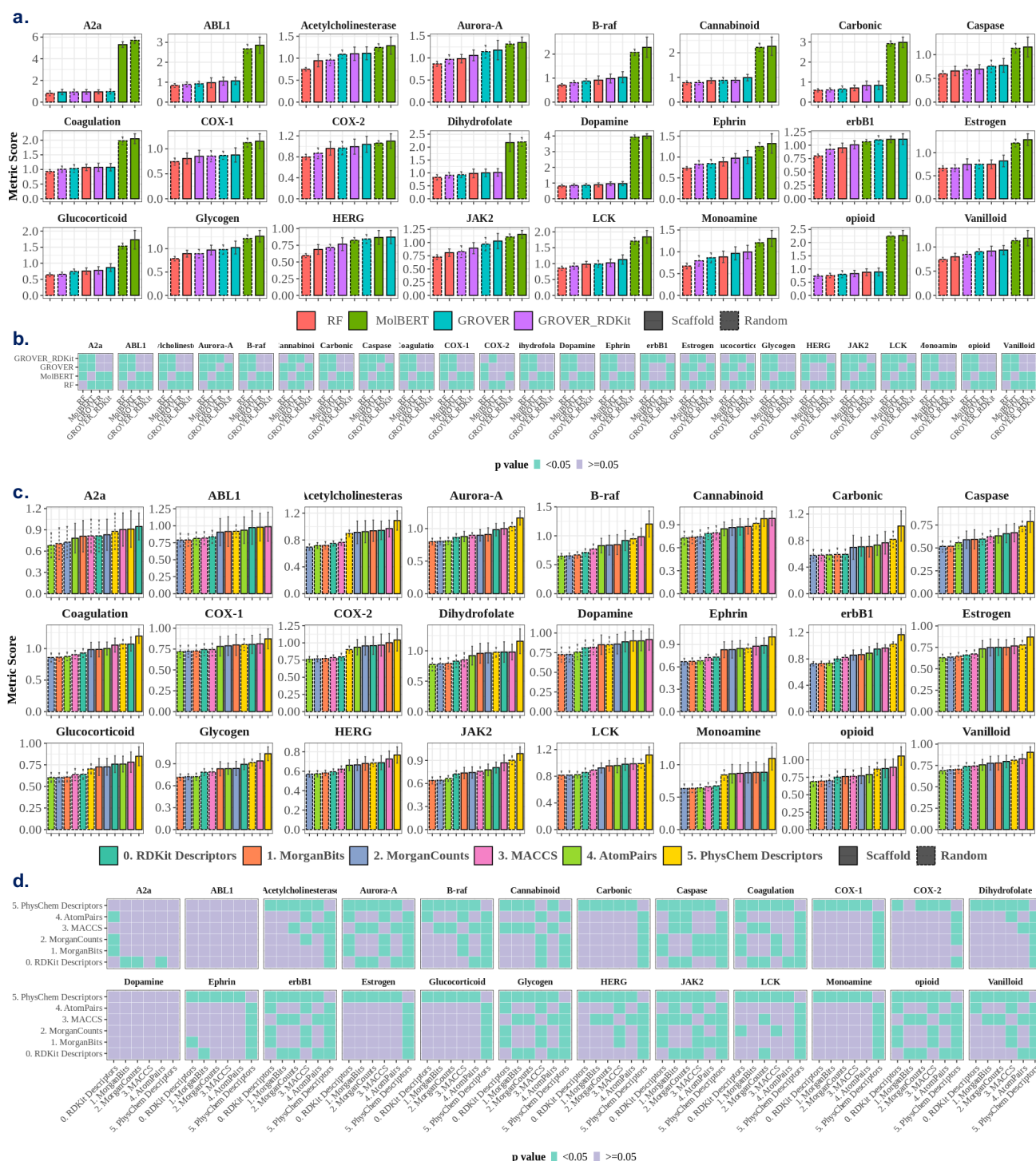


Figure 10. Performance in Datasets by Cortés-Ciriano et al (errorbar: standard deviation). (a). Performance of RF on RDKit2D descriptors, MolBERT, GROVER and GROVER_RDKit. (b). Mann-Whitney U significance for plot **a** under scaffold split. (c). Performance of RF on fixed representations. (d). Mann-Whitney U significance for plot **c** under scaffold split.

and in CYP2D6, AUPRC is nearly zero. If plotting AUPRC against AUROC or PPV (Sup. Figure 18c&d), AUROC can exaggerate prediction performance, especially in CYP2D6

and CYP3A4. Thus, AUROC can be over-optimistic. Furthermore, despite the high AUROC (c.a. 0.90), AUPRC (c.a. 1.0) and PPV (c.a. 0.90) in BBBP, NPV drops to c.a. 0.75 for RF

and c.a. 0.65 for the other three models (Figure 7b). In this case, despite the nearly perfect collective metrics, namely AUROC and AUPRC, NPV can be very limited. This can be an issue if the goal of virtual screening is to identify hits impermeable through the blood-brain barrier, since only around 65% are truly not permeable among the predicted negatives. On the contrary, although the highest AUROC in HIV can reach c.a. 0.80, its best PPV is below 0.25 (Figure 7b). Similarly, PPV is limited for the opioids-related datasets (Figure 9b). For instance, the best PPV is c.a. 0.7 in MDR1, whereas in MOR, DOR and KOR, it is around 0.6, let alone in highly imbalanced CYP2D6 and CYP3A4, where PPV can drop to nearly zero. Thus, if the goal of virtual screening is to identify hits active towards these targets, a large proportion of the predicted actives can be false positives. In short, precision metrics can be more suitable for evaluating prediction performance at classification setting, which is further contingent upon the emphasis on positives or negatives, i.e., the specific goal of virtual screening.

4.2.5 Regression vs Classification: which is more proper?

To study how task setting affects prediction performance, we set both regression and classification settings for the opioids-related datasets (Figures 8b & 9b). As shown in Figure 9b, at classification setting, all models achieve limited performance in CYP2D6, with particularly abysmal performance in PPV. However, under regression setting, RMSE and MAE in CYP2D6 can be lowered to c.a. 1.5, which suggests that regression might be more suitable for CYP2D6, although the pIC50 labels can be noisy⁶³. On the contrary, in MDR1, MOR, DOR and KOR where the prediction performance is promising indicated by high AUROC at classification setting, the regression error, as indicated by RMSE and MAE, are c.a. 2.0. One potential cause for the disparate performance between the classification and regression settings could be the arbitrary activity cutoff. As shown in Sup. Figure 12c, classification performance (RF on MorganBits fingerprints) varies with the cutoff values. Since each dataset has a unique label distribution (Figure 6), the cutoff value at 6 may cause prediction difficulty to different extents. For instance, similar molecular structures with close pIC50 values around 6 could be coerced to actives vs. inactives, which forms a challenging task and may act as a major source of misclassification.

In fact, these molecules are the so-called "edge cases"⁶³, which are defined as molecules in the same scaffold but with pIC50 values spanning from 5 to 7 in this study. The percentages of edge-case molecules in the test sets are shown in Figure 9g. For MOR, DOR and KOR, c.a. 5% of molecules are edge cases. For CYP2D6 and CYP3A4, the edge cases are c.a. 1%, presumably due to very few molecules with pIC50 above 5 (Figure 6b). We also calculated classification performance with edge-case molecules removed in the test sets (Figure 9h). Results showed that classification performance tend to increase after edge-case removal, especially for MOR, DOR and KOR, suggesting the challenge posed by edge cases. We further plotted prediction errors (predicted value - label

value) vs label values at regression setting (RF on Morgan-Bits). In Figure 9i, prediction error is not constant across the label values range. Instead, there exists an increasing trend, which suggests that for molecules with high pIC50 values, the model is prone to overestimation and for molecules with low pIC50 values, underestimation is more likely to happen. For CYP2D6, prediction errors are mostly around zero, which explains the relatively low RMSE. For all edge cases, prediction errors are mostly positive, which indicates that the model tends to overestimate their pIC50.

To further examine the effect of activity cutoff values, we plotted the distribution of predicted probabilities for edge-case molecules at different cutoff settings. For MOR, DOR and KOR, the predicted probabilities are shifted to the left when the cutoff value increases from 5 to 7 (Figure 9j), suggesting these edge cases are more likely to be predicted as inactive. Nonetheless, for edge cases in MDR1, CYP2D6 and CYP3A4, the predicted probabilities are all near zero, regardless of the cutoff values, which may be attributed to the data-imbalance issue. Since most training examples are negative, the model would hardly learn to correctly predict positive instances. One practical implication is that positive ratios should be checked when selecting a cutoff value. If the binarized dataset is highly imbalanced, directly regressing on the labels is recommended, based on our observations with the CYP2D6 dataset.

Nonetheless, it is noteworthy that pIC50 labels still have inherent noise, which is often heteroscedastic⁶³. One example given is that pIC50 of 5.1 or 4.9 are often treated equally important in contributing to the opposing activity (e.g., classification threshold of 5). However, the accuracy of such measurements may not be 100% guaranteed in the presence of experimental errors, which can be categorized into systematic error and random error⁷⁵. Systematic error is hard to trace down whereas random error can be approximated by a Gaussian distribution. A previous work by Cortés-Ciriano et al⁷⁶ simulated adding random noise to pIC50 values in 12 datasets and assessed how it affects subsequent predictive performance of 12 models. Results showed that different models showed different sensitivity to the added noise. Other factors underlying the response to noise include noise levels and noise distribution, which is further dependent on the label distribution of a specific dataset and the cutoff values.

4.3 On the chemical space generalization

4.3.1 Inter-scaffolds generalization

As illustrated in Figure 4, we conducted experiments using all models under in the opioids-related datasets at regression setting. Prediction performance are summarized in Figure 8d (scaffold split) and Sup. Figure 16b (random split). Given no scaffolds overlap among training, validation and test sets under scaffold split, we contrasted the prediction performance between scaffold and random split so as to evaluate how the models perform during the inter-scaffold generalization. The difference of mean RMSE between random split and scaffold split is shown in Figure 11a. Note that

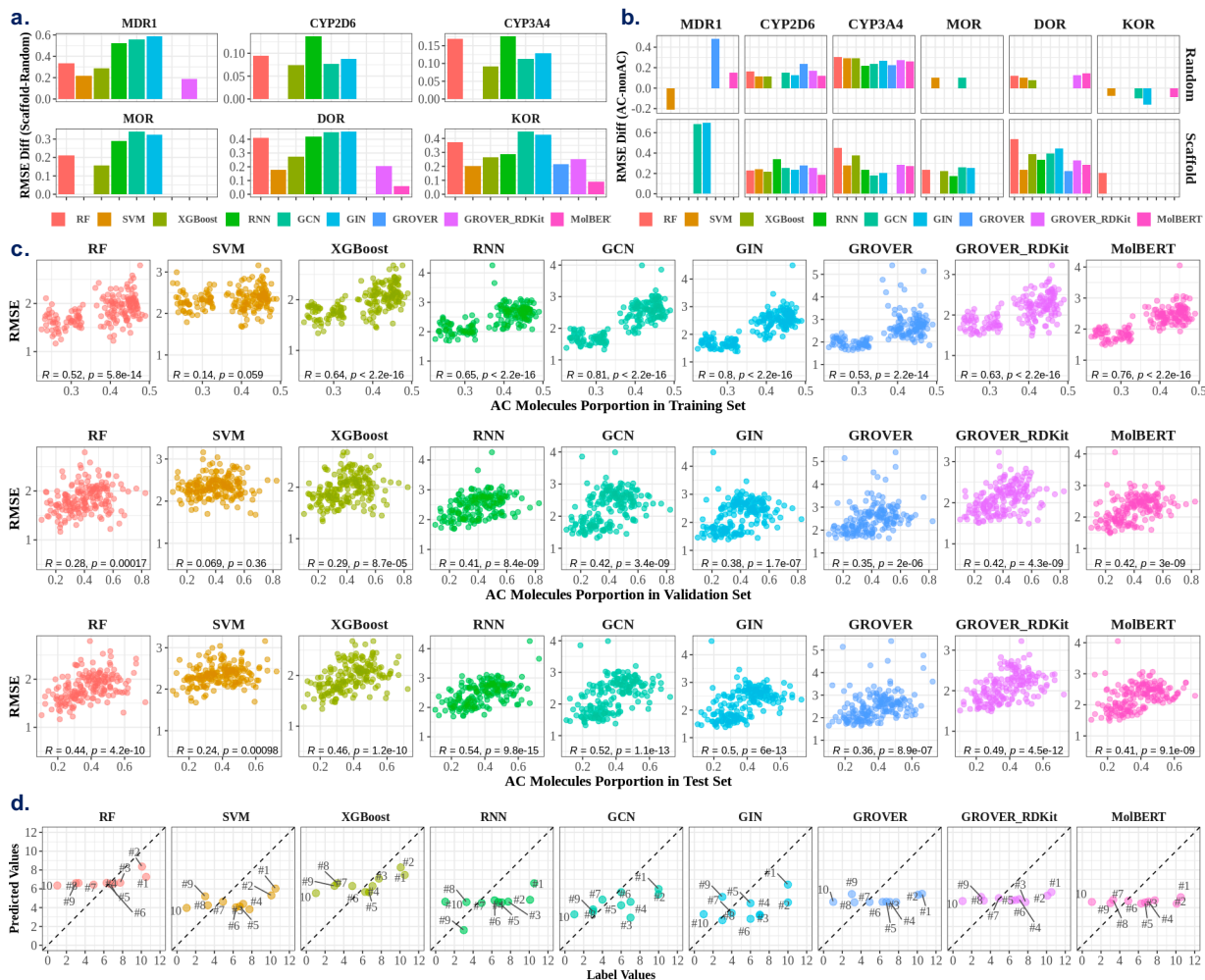


Figure 11. Chemical Space Generalization Check on Prediction Performance in Opioids-related Datasets at Regression Setting. **a.** RMSE difference between scaffold and random split. **b.** RMSE difference between for AC and non-AC molecules scaffold and random split. **c.** Relationship between RMSE and AC Molecules Proportions. **d.** Raw Predictions for AC showcase molecules (Figure 6c).

we also conducted Mann-Whitney U test here: if there is no statistical significance in the difference, it is imputed as zero. Compared to random split, prediction performance are worse under scaffold split (significantly higher RMSE) in all opioids-related datasets using most models. This observation manifests the inter-scaffold generalization challenge. Notably, using MolBERT or GROVER_RDKit, prediction performance difference can be negligible between split and scaffold split in MDR1, CYP2D6, CYP3A4, MOR and DOR. Using GROVER, the differences of prediction performance are all zero, which could be due to the high variability associated with GROVER’s performance (Figure 12a). Nonetheless, given the limited performance of pretrained models under scaffold split (see Section 4.2), it does not suffice to claim achieving the inter-scaffold generalization.

Besides the difference in metric means, we also observed that metric variability is also higher under scaffold split across

all models (Figure 12a), indicating higher uncertainty in prediction during inter-scaffold generalization.

4.3.2 Intra-scaffold generalization

To examine the intra-scaffold generalization, we contrasted prediction performance for AC and non-AC molecules (see Section 4.1.2) under both scaffold and random split. Mann-Whitney U test is conducted to examine the statistical significance and non-significant differences are imputed as zero.

As shown in Figure 11b, RMSE is generally higher for AC molecules. The inferior performance for the AC molecules suggests the limited intra-scaffold generalization in the case of activity cliffs. Besides, the performance differences between AC and non-AC molecules are generally more frequently observed under scaffold split. In other words, random split can alleviate the intra-scaffold generalization in the case of activity cliffs, presumably due to that some AC scaffolds have been

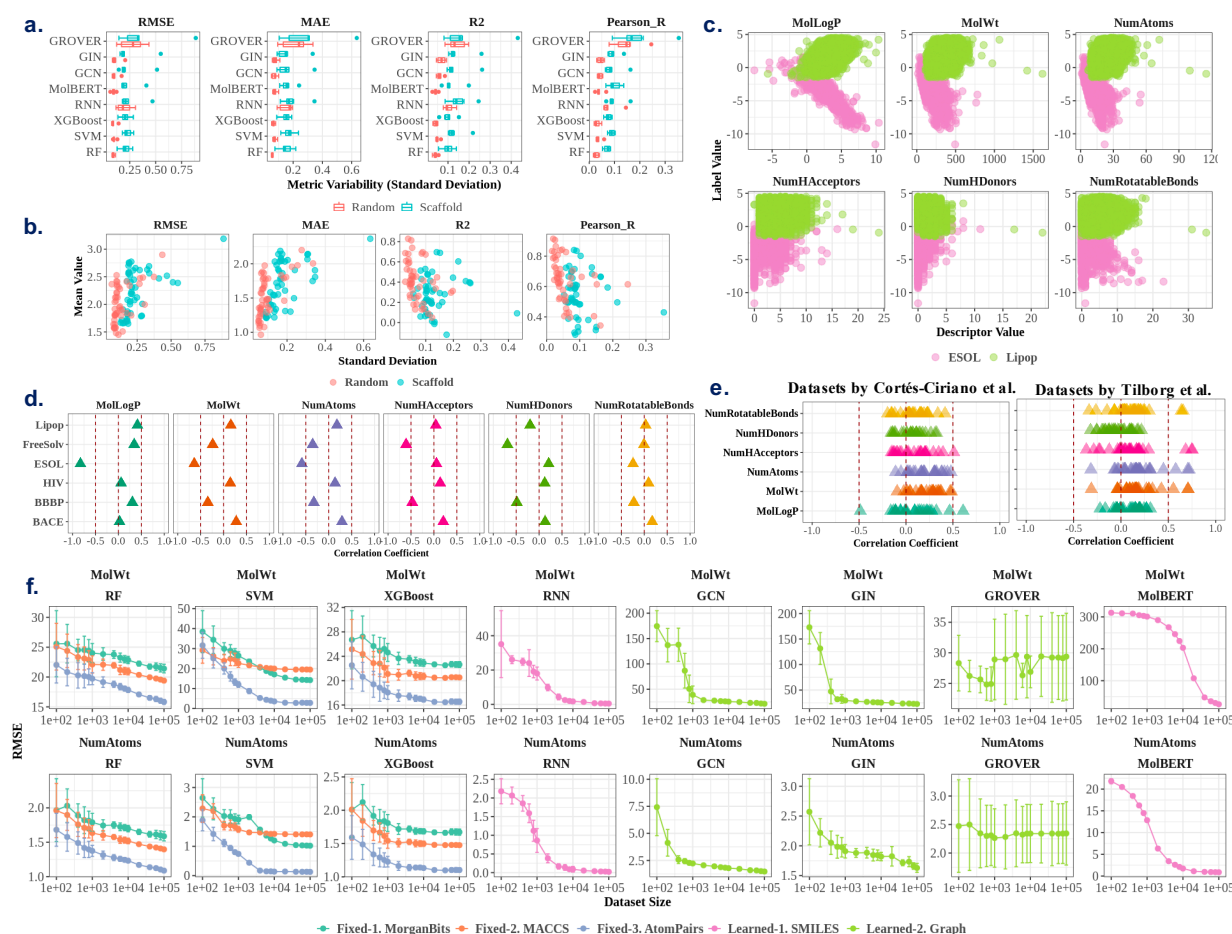


Figure 12. Exploration into Molecular Property Prediction Performance (a). Metric variability for RF on fixed representations in opioids-related datasets (b). Relationship between label value and molecular descriptors (c). Correlation coefficient between label value and molecular descriptors in MoleculeNet benchmark datasets (d). Correlation coefficient between label value and molecular descriptors in activity datasets by Cortés-Ciriano et al. and Tilborg et al. (e) Prediction performance in descriptors datasets with varying dataset sizes

seen during training, which enables better prediction at inference time. Again, this observation highlights the importance of scaffolds in molecular property prediction.

Moreover, we plotted RMSE against the proportion of AC molecules in the training/validation/test sets (Figure 11c). RMSE values tend to be higher when the proportions of AC molecules increase, especially in the training set. The strong positive correlations suggests activity cliffs is a key factor in limited prediction performance. One exception is SVM, where this correlation is weak. In addition, we also examined the learned representations for the AC showcase molecules (Figure 6c) under scaffold split (seed: 4). As shown in Figure 11d, the predicted pIC50 values are not well aligned with the $y = x$ line. For MolBERT, GROVER and GROVER_RDKit, results are especially abysmal, where the average pIC50 seem to be simply imputed as the predicted values for the AC molecules.

In fact, as pointed out by Robinson *et al.*¹⁷, active molecules with different scaffolds can interact with the target with very

different mechanisms. Thus, expecting a model to generalize by learning from unseen scaffolds can be somewhat unrealistic. Here, by interrogating the intra-scaffold generalization, we further substantiate this point with the activity-cliffs issue, which has two-fold meanings: 1). exposing the predictive model to a set of diverse scaffolds during training phase may be conducive for inference, even holding potential for activity cliffs, although further study is needed; 2). when applying a trained molecular property prediction model, for example, in a deep reinforcement learning framework for drug design⁷⁷, if the generated molecule has a novel scaffold, which is further related to molecules with drastic activity changes, the prediction should be noted with lower certainty.

Furthermore, to find out the best performing model in the case of activity cliffs, we applied RF, SVM and XGBoost on fixed molecular representations in the activity datasets proposed by Tilborg et al²⁴. As shown in Sup. Figure 19, RF on MorganBits, MorganCounts or AtomPairs fingerprints

generally achieves lowest RMSE whereas SVM on PhysChem descriptors shows worst performance mostly.

4.4 Why representation learning models fail?

Based on the extensive experimentation and rigorous comparison, we observed that traditional machine learning models on fixed molecular representations are very powerful in molecular property prediction, outperforming representation learning models in most datasets. Thus, one natural question is: why representation learning models fail? In this section, we further analyzed prediction results and conducted follow-up experiments to highlight some pertinent observations.

4.4.1 Metric variability correlates with performance.

In Figure 12a, we plotted the standard deviation of all regression metrics in opioids-related datasets for different models. In addition to the varying prediction performance as discussed in Section 4.2, metric variability also varies across models. Representation learning models like GROVER, in particular, exhibit high variability in all metrics. Moreover, metric variability can be further correlated with mean metric values. As shown in Figure 12b, RMSE and MAE (the higher, the worse) tend to go up when metric variability increases whereas R2 and Pearson_R go down (the lower, the worse) with higher metric variability. The inherent variability underlying representation learning models can be a manifestation of the prediction performance, which also suggest the importance of reporting metric variability along with mean values. Notably, imbalanced datasets can be a cause for the high variability, and as a result, low performance. For instance, in CYP2D6 at classification setting (positive rate: 1.4%), all models exhibit highly variant yet very limited performance with mean AUROC around 0.5, or even lower.

4.4.2 Descriptors correlate with molecular properties.

In Section 4.2, we observed that molecular descriptors can be particularly powerful in certain datasets. For instance, RF on the PhysChem descriptors can achieve comparable performance with the best-performing RDKit2D descriptors in ESOL. On the contrary, biological activity is more complicated and cannot be well tackled with the descriptors and structural fingerprints are more powerful (Figures 8e & 10c).

To explain why PhysChem descriptors show such high performance, we plotted the labels against some selected descriptors for ESOL and Lipop. As depicted in Figure 12c, MolLogP has a linear relationship with ESOL's label whereas Lipop does not exhibit strong correlation patterns. To quantify the relationship, we calculated the correlation coefficients between molecular properties and PhysChem descriptors in the benchmark datasets (Figure 12d). For ESOL, the coefficient with MolLogP is nearly -1, which is very likely to be the reason why PhysChem descriptors excel in its prediction. Among other benchmark datasets, FreeSolv also exhibit moderate correlation with multiple descriptors, such as MolLogP, NumAtoms, NumHAcceptors and NumHDonors, the coefficients of which range from -0.75 to -0.5. This observation

may explain why PhysChem descriptors are among the top 3 best performing molecular representations (Figure 7e).

We also conducted correlation analysis for the activity datasets proposed by Cortés-Ciriano et al and Tilborg et al. As shown in Figure 12e, coefficients in most datasets are within -0.5 and 0.5, suggesting weak correlation between binding activity and the descriptors. This could be why PhysChem descriptors shows limited performance in activity prediction (Figure 10c & Sup. Figure 19). Notably, MolWt, NumAtoms and NumHAcceptors and NumRotatableBonds show moderate correlation with activity in certain datasets (correlation coefficient greater than 0.5) whereas, surprisingly, NumHDonors is weakly correlated with activity.

4.4.3 Prediction performance varies with dataset size.

Given the advantage of descriptors in certain datasets over representation learning models, we assembled the descriptor datasets for the prediction of MolWt and NumAtoms (Figure 5b), which is a further interrogation on the basic predictive power. Moreover, unlike the public activity datasets which often have limited dataset sizes, descriptors datasets can be assembled at low costs. In total, we built 16 datasets with varying sizes for each descriptor, which are further split into training, validation and test sets under scaffold split.

As shown in Figure 12e, when dataset size is less than 1000, prediction for MolWt can have large variability across all models. Even with fixed representations like MorganBits, MACCS and AtomPairs, mean RMSE can be around 25 for RF, 40 for SVM and 30 for XGBoost, with high variability as well. For sequence-based models, RNN has RMSE around 40 when dataset size is 100 whereas MolBERT has RMSE around 300, which is the highest error among all. For graph-based models, GCN and GIN show RMSE around 200 when dataset size is 100 whereas GROVER can achieve RMSE around 30, similar to the performance of fixed representations. This manifests the predictive power of pretrained GROVER to some extent. Moreover, when dataset size increases from 100 to 1000, we can see that RMSE of GCN and GIN decreases by around 75%, lowered to below 50. For GROVER, although RMSE also decreases from size 100 to 1000, the trend is not as obvious, though. For RNN, RMSE decreases by around 50% to below 20. However, there is little difference for MolBERT. Overall, the mean and variance of RMSE is decreasing with the increasing dataset size. When dataset size keeps increasing from 1000 to 100K, the RMSE of RF can decrease to around 15, similar to XGBoost. Surprisingly, SVM achieves nearly perfect RMSE to around zero. We speculate that SVM, despite its inferior performance when dataset size is small, it can achieve superior performance when dataset size is large. Also, we found that the best-performing representation is AtomPairs, followed by MACCS and MorganBits. Notably, morganBits can outperform MACCS when used with SVM. For representation learning models, we observed that RMSE of RNN drastically decreases from 20 to nearly zero, whereas GCN and GIN drop to around 10.

For the prediction of MolWt and NumAtoms, we found

that AtomPairs is a powerful fixed representation (especially if used with SVM) and the performance of RF, SVM and XG-Boost has an improvement trend with increasing dataset size. For the representation learning models, regular neural network models can have limited performance when dataset size is below 1000, where pretrained graph-based model GROVER shows superior performance, which is consistent with observations in Section 4.2, where GROVER achieves quite good performance in FreeSolv (dataset size: 642). Surprisingly, pretrained sequence-based model MolBERT shows very limited performance, i.e., RMSE over 200, when dataset size is less than 10K. Nonetheless, MolBERT shows significant decreasing trend when dataset size is greater than 10K (Sup. Figure 20) whereas GROVER's performance does not improve much with the increasing dataset size. Eventually, RNN achieves best performance when dataset size is greater than 10K, which manifests the promise of representation learning models in the "big-data" space. Still, activity datasets can be quite limited, especially those from public databases, which can be another reason why representation learning models fail at times.

Discussion

In this study, we take a respite from representation learning for molecular property prediction. We conducted a comprehensive evaluation to interrogate fundamentals underlying molecular property prediction. A collection of models, including traditional machine learning models and neural network models, and a set of molecular representations were evaluated on MoleculeNet benchmark datasets, opioids-related datasets, other activity datasets and descriptor datasets. In total, we trained over 60,000 models. Notably, two large models based on SMILES strings and molecular graphs, i.e., MolBERT¹¹ and GROVER¹³ were carefully investigated, both of which have transformer as the core unit and adopted self-supervised learning for pretraining.

Compared to supervised learning, self-supervised learning does not require heavy human annotations⁷⁸, which can be particularly expensive in drug discovery¹. As shown in the work by Hu *et al.*¹², self-supervised pre-training helps avoid the negative transfer associated with supervised pre-training. Self-supervised learning can be roughly categorized into: generative, contrastive and generative-contrastive (adversarial)⁷⁹. Pretraining tasks, such as masked language modeling in MolBERT and contextual property prediction in GROVER, are leaning towards the generative type. Recently, the contrastive type of self-supervised pretraining has also been applied in molecular property prediction. For example, MolCLR¹⁴ proposes three augmentation strategies, namely, atom masking, bond deletion and subgraph removal, on molecular graphs to pretrain GCN and GIN, respectively. More recently, iMolCLR¹⁵ has also been proposed, where structural similarities between negative pairs and fragment-level contrasting substructures decomposed from molecules are integrated into the NT-Xent loss function. Notably, one pretraining task in MolBERT¹¹ is the SMILES equivalence prediction, where

given an input of two SMILES strings (the second SMILES is either randomly sampled from the pretraining corpus or an equivalent SMILES), the model predicts whether they represent the same molecule. Based on the ablation study, however, the SMILES equivalence task slightly but consistently decreases downstream performance. Besides, MolBERT¹¹ and GROVER¹³ also utilized RDKit⁴⁸ to calculate molecular descriptors values or extract graph-level motifs as domain-relevant labels for pretraining. As indicated by the ablation study in MolBERT, molecular descriptors values prediction has the highest impact on downstream performance. Also shown in this study, RDKit2D descriptors play a crucial role in GROVER and moreover, fixed representations such as RDKit2D descriptors significantly outperform the learned representations in many datasets, which coincides with previous studies^{42,80}. One potential direction would be designing more suitable ways of exploiting fixed representations.

Nonetheless, despite the advancement in AI techniques, whether AI can benefit real-world drug discovery is not without its concerns^{25,26}. Guidelines for evaluating molecules generated by AI techniques have been suggested by Walters *et al.*⁸¹. Likewise, evaluation of molecular property prediction should also be standardized. Recently, Bender *et al.*⁸² proposed a set of evaluation guidelines for machine learning tools, covering appropriate comparison methods and evaluation metrics, among others. In this study, we addressed molecular property prediction from three aspects: datasets profiling, model evaluation and chemical space generalization (Figure 1). For the datasets, each of them has unique label distribution and molecular structures, which poses different degrees of prediction difficulty. The molecular structures are dissected into scaffolds and structural traits, including fragments (functional groups and heterocycles) and other structural traits, such as MolWt and NumAtoms. Furthermore, under different dataset split schemes and with different seeds, the structural and label divergence among the training, validation and test sets also vary, which acts as a source for the performance variance. For the model evaluation, we compared a collection of models, including three machine learning models, three regular neural network models and two large models pretrained with self-supervised learning strategies, on different molecular representations. With rigorous statistical analyses, fixed representations are shown to lead in the performance in most datasets, suggesting there is still room for further advancing representation learning for molecular property prediction. For the chemical space generalization, we dissect it into inter-scaffold generalization and intra-scaffold generalization. The inferior prediction performance under scaffold split (compared to random split) suggests that better AI techniques are needed to improve w.r.t. inter-scaffold generalization. Similarly, the inferior performance for the AC molecules (see Section 2.4.3) suggests more efforts are needed for intra-scaffold generalization, especially in the case of activity cliffs. Routine evaluation on activity-cliffs is needed, which is missing in many previous studies. One reason for the

neglect of this issue could be due to the heavy reliance on the MoleculeNet benchmark datasets.

Indeed, the widely-used benchmark datasets may be of little relevance to real-world drug discovery¹⁸. Some benchmark datasets can pose unreasonable prediction tasks²⁶. For example, SIDER¹⁶ is a dataset for 1,427 marketed drugs and their side effects in 27 system organ classes. In addition to the molecular structures, there are many other factors underlying the side effects in humans, such as food-drug interactions⁸³, drug-drug interactions⁶², among others²⁶. Thus, it is unrealistic to expect a model to directly predict side effects from the chemical structures. Another example is ClinTox¹⁶, which has a classification task for FDA approval status in addition to the clinical trial toxicity. These two tasks can only be partially attributed to the chemical structures. Thus, to examine the usefulness of the advanced representation learning models, we also assembled a suite of opioids-related datasets from ChEMBL. As shown in Figure 6, the MOR, DOR and KOR datasets related to the PD aspect of opioid overdose are quite balanced. On the contrary, the CYP2D6 and CYP3A4 datasets related to the PK aspect of opioid overdose are extremely skewed to the left with an active rate less than 10% under the cutoff 6. Consequently, the PPV for these two metabolic enzymes is very limited. Indeed, the datasets in some domains are still lacking²⁶. Besides, these activity datasets from public databases can be very noisy. For example, we found quite some duplicates and contradictory records in the opioids-related datasets, which were removed from further analysis. Sometimes, even the established benchmark datasets need an extra “washing” step to ensure the data quality⁴².

Given the limited prediction performance, we also explored into potential explanations on why representation learning fails and discussed some pertinent facts around the worse performance of molecular representation learning models. Firstly, presumably due to large numbers of parameters, representation learning models generally show greater metric variability, which is further negatively correlated with metric mean values. Secondly, some molecular properties show correlations with certain molecular descriptors, which leads to superior performance of the fixed representations. Thirdly, nevertheless, by experimenting on the assembled descriptor datasets with varying dataset sizes, we found that representation learning models cannot accurately predict simple molecular descriptors, especially when dataset size is small. One exception, though, is that pretrained GROVER performs comparably well with fixed representations when data points are less than 1,000. However, GROVER’s performance does not improve with the increasing dataset sizes. On the other hand, traditional machine learning models and regular neural network models exhibit lower prediction error when there are more data points. Particularly, RNN starts to achieve best performance when dataset size reaches 6,000. For pretrained MolBERT, it exhibits little advantage when descriptor datasets have small sizes. However, when dataset size reaches 100,000, it shows comparable performance with the fixed representations. The

dataset size can be key bottleneck. More efforts are needed in high-quality datasets so as to exert the power of representation learning models.

Last but not least, there are still some limitations in this study. Firstly, the sources underlying molecular property prediction include dataset split uncertainty, experimental data uncertainty, and model training uncertainty⁶³. Our experimental scheme of repeating datasets split 30 times with different random seeds only partially addresses the uncertainty. Moreover, there could also be variations introduced during model training, such as random weight initialization and random mini-batch shuffling⁸⁴. As a result, the ensembling technique has been proposed to alleviate the uncertainty related to model training and improve prediction accuracy⁸, which was not evaluated in this study due to heavy computation burden. Another underlying assumption, yet often neglected, is that the collected datasets are usually regarded as the gold standard without any experimental errors, which, however, may not hold true. Experimental uncertainty needs to be taken into consideration as well⁶³. Secondly, the explainability of the molecular property prediction models is not covered in this study, which is related to the explainable AI, aiming to make the predictions more understandable by domain experts⁸⁵.

In conclusion, we expect that by taking this respite, awareness of the fundamentals underlying molecular property prediction can be raised, which will eventually bring even better AI techniques for molecule property prediction.

References

1. Wouters, O. J., McKee, M. & Luyten, J. Estimated research and development investment needed to bring a new medicine to market, 2009-2018. *JAMA* **323**, 844–853 (2020).
2. Simoens, S. & Huys, I. R&d costs of new medicines: A landscape analysis. *Front. Med.* **8** (2021).
3. Chen, H., Engkvist, O., Wang, Y., Olivecrona, M. & Blaschke, T. The rise of deep learning in drug discovery. *Drug Discov. Today* **23**, 1241–1250 (2018).
4. Vamathevan, J. *et al.* Applications of machine learning in drug discovery and development. *Nat. Rev. Drug Discov.* **18**, 463–477 (2019).
5. Deng, J., Yang, Z., Ojima, I., Samaras, D. & Wang, F. Artificial intelligence in drug discovery: applications and techniques. *Brief. Bioinforma.* **23**, bbab430 (2022).
6. David, L., Thakkar, A., Mercado, R. & Engkvist, O. Molecular representations in ai-driven drug discovery: a review and practical guide. *J. Cheminformatics* **12**, 1–22 (2020).
7. Mayr, A. *et al.* Large-scale comparison of machine learning methods for drug target prediction on chembl. *Chem. Sci* **9**, 5441–5451 (2018).

8. Yang, K. *et al.* Analyzing learned molecular representations for property prediction. *J. Chem. Inf. Model.* **59**, 3370–3388 (2019).
9. Honda, S., Shi, S. & Ueda, H. R. Smiles transformer: pre-trained molecular fingerprint for low data drug discovery. *arXiv preprint arXiv:1911.04738* (2019).
10. Chithrananda, S., Grand, G. & Ramsundar, B. Chemberta: Large-scale self-supervised pretraining for molecular property prediction. *arXiv preprint arXiv:2010.09885* (2020).
11. Fabian, B. *et al.* Molecular representation learning with language models and domain-relevant auxiliary tasks. *arXiv preprint arXiv:2011.13230* (2020).
12. Hu, W. *et al.* Strategies for pre-training graph neural networks. *arXiv preprint arXiv:1905.12265* (2019).
13. Rong, Y. *et al.* Grover: Self-supervised message passing transformer on large-scale molecular data. *arXiv preprint arXiv:2007.02835* (2020).
14. Wang, Y., Wang, J., Cao, Z. & Farimani, A. B. Molclr: Molecular contrastive learning of representations via graph neural networks. *arXiv preprint arXiv:2102.10056* (2021).
15. Wang, Y., Magar, R., Liang, C. & Barati Farimani, A. Improving molecular contrastive learning via faulty negative mitigation and decomposed fragment contrast. *J. Chem. Inf. Model.* (2022).
16. Wu, Z. *et al.* Moleculenet: a benchmark for molecular machine learning. *Chem. Sci* **9**, 513–530 (2018).
17. Robinson, M. C., Glen, R. C. *et al.* Validating the validation: reanalyzing a large-scale comparison of deep learning and machine learning models for bioactivity prediction. *J. Comput. Aided Mol.* 1–14 (2020).
18. Walters, W. P. & Barzilay, R. Critical assessment of ai in drug discovery. *Expert. Opin Drug Discov* 1–11 (2021).
19. Shen, W. X. *et al.* Out-of-the-box deep learning prediction of pharmaceutical properties by broadly learned knowledge-based molecular representations. *Nat. Mach. Intell.* **3**, 334–343 (2021).
20. Xiong, Z. *et al.* Pushing the boundaries of molecular representation for drug discovery with the graph attention mechanism. *J. Med. Chem.* **63**, 8749–8760 (2019).
21. Na, G. S., Chang, H. & Kim, H. W. Machine-guided representation for accurate graph-based molecular machine learning. *Phys. Chem. Chem. Phys.* **22**, 18526–18535 (2020).
22. Mendez, D. *et al.* ChEMBL: towards direct deposition of bioassay data. *Nucleic Acids Res.* **47**, D930–D940 (2019).
23. Cortés-Ciriano, I. & Bender, A. Deep confidence: a computationally efficient framework for calculating reliable prediction errors for deep neural networks. *J. chemical information modeling* **59**, 1269–1281 (2018).
24. van Tilborg, D., Alenicheva, A. & Grisoni, F. Exposing the limitations of molecular machine learning with activity cliffs. *J. Chem. Inf. Model.* **62**, 5938–5951 (2022).
25. Bender, A. & Cortes-Ciriano, I. Artificial intelligence in drug discovery: what is realistic, what are illusions? part 1: Ways to make an impact, and why we are not there yet. *Drug Discov. Today* (2020).
26. Bender, A. & Cortes-Ciriano, I. Artificial intelligence in drug discovery: what is realistic, what are illusions? part 2: a discussion of chemical and biological data used for ai in drug discovery. *Drug Discov. Today* (2021).
27. Gao, K. *et al.* Are 2d fingerprints still valuable for drug discovery? *Phys. Chem. Chem. Phys.* **22**, 8373–8390 (2020).
28. Morgan, H. L. The generation of a unique machine description for chemical structures—a technique developed at chemical abstracts service. *J. Chem. Doc* **5**, 107–113 (1965).
29. Rogers, D. & Hahn, M. Extended-connectivity fingerprints. *J. Chem. Inf. Model.* **50**, 742–754 (2010).
30. Skinnider, M. A., Stacey, R. G., Wishart, D. S. & Foster, L. J. Deep generative models enable navigation in sparsely populated chemical space. *Nat Mach Intell* (2021).
31. Capecchi, A., Probst, D. & Reymond, J.-L. One molecular fingerprint to rule them all: drugs, biomolecules, and the metabolome. *J. cheminformatics* **12**, 1–15 (2020).
32. Weininger, D. Smiles, a chemical language and information system. 1. introduction to methodology and encoding rules. *J Chem Inf. Comput. Sci* **28**, 31–36 (1988).
33. Weininger, D., Weininger, A. & Weininger, J. L. Smiles. 2. algorithm for generation of unique smiles notation. *J Chem Inf. Comput. Sci* **29**, 97–101 (1989).
34. Goh, G. B., Hodas, N. O., Siegel, C. & Vishnu, A. Smiles2vec: An interpretable general-purpose deep neural network for predicting chemical properties. *arXiv preprint arXiv:1712.02034* (2017).
35. Kipf, T. N. & Welling, M. Semi-supervised classification with graph convolutional networks. *arXiv preprint arXiv:1609.02907* (2016).
36. Veličković, P. *et al.* Graph attention networks. *arXiv preprint arXiv:1710.10903* (2017).
37. Gilmer, J., Schoenholz, S. S., Riley, P. F., Vinyals, O. & Dahl, G. E. Neural message passing for quantum chemistry. In *ICML*, 1263–1272 (PMLR, 2017).
38. Xu, K., Hu, W., Leskovec, J. & Jegelka, S. How powerful are graph neural networks? *arXiv preprint arXiv:1810.00826* (2018).

39. Breiman, L. Random forests. *Mach. learning* **45**, 5–32 (2001).
40. Chen, T. & Guestrin, C. Xgboost: A scalable tree boosting system. In *Proceedings of the 22nd acm sigkdd international conference on knowledge discovery and data mining*, 785–794 (2016).
41. Cortes, C. & Vapnik, V. Support-vector networks. *Mach. learning* **20**, 273–297 (1995).
42. Jiang, D. *et al.* Could graph neural networks learn better molecular representation for drug discovery? a comparison study of descriptor-based and graph-based models. *J. Cheminformatics* **13**, 1–23 (2021).
43. Cho, K., Van Merriënboer, B., Bahdanau, D. & Bengio, Y. On the properties of neural machine translation: Encoder-decoder approaches. *arXiv preprint arXiv:1409.1259* (2014).
44. Chung, J., Gulcehre, C., Cho, K. & Bengio, Y. Empirical evaluation of gated recurrent neural networks on sequence modeling. *arXiv preprint arXiv:1412.3555* (2014).
45. Devlin, J., Chang, M.-W., Lee, K. & Toutanova, K. Bert: Pre-training of deep bidirectional transformers for language understanding. *arXiv preprint arXiv:1810.04805* (2018).
46. Shaw, P., Uszkoreit, J. & Vaswani, A. Self-attention with relative position representations. In *Proceedings of the 2018 Conference of the North American Chapter of the Association for Computational Linguistics: Human Language Technologies, Volume 2 (Short Papers)*, 464–468, DOI: [10.18653/v1/N18-2074](https://doi.org/10.18653/v1/N18-2074) (Association for Computational Linguistics, New Orleans, Louisiana, 2018).
47. Wieder, O. *et al.* A compact review of molecular property prediction with graph neural networks. *Drug Discov. Today* **37**, 1–12 (2020).
48. Landrum, G. Rdkit: Open-source cheminformatics software. *RDKit* (2016).
49. for Disease Control, C., Prevention *et al.* Drug overdose deaths in the united states, 1999–2018. *NCHS Data Brief: Natl. Cent. for Heal. Stat.* (2020).
50. Yaksh, T. L., Hunt, M. A. & Dos Santos, G. G. Development of new analgesics: an answer to opioid epidemic. *Trends Pharmacol. Sci.* **39**, 1000–1002 (2018).
51. Deng, J. *et al.* A large-scale observational study on the temporal trends and risk factors of opioid overdose: Real-world evidence for better opioids. *Drugs-Real World Outcomes* 1–14 (2021).
52. Sterling, T. & Irwin, J. J. Zinc 15–ligand discovery for everyone. *J. Chem. Inf. Model.* **55**, 2324–2337 (2015).
53. Saito, T. & Rehmsmeier, M. The precision-recall plot is more informative than the roc plot when evaluating binary classifiers on imbalanced datasets. *PloS one* **10**, e0118432 (2015).
54. Jenkins, J. L., Bender, A. & Davies, J. W. In silico target fishing: Predicting biological targets from chemical structure. *Drug Discov. Today Technol.* **3**, 413–421 (2006).
55. Hu, Y. & Bajorath, J. What is the likelihood of an active compound to be promiscuous? systematic assessment of compound promiscuity on the basis of pubchem confirmatory bioassay data. *AAPS J.* **15**, 808–815 (2013).
56. Wale, N. & Karypis, G. Target fishing for chemical compounds using target-ligand activity data and ranking based methods. *J. Chem. Inf. Model.* **49**, 2190–2201 (2009).
57. Patrick Walters, W. Comparing classification models—a practical tutorial. *J. Comput. Aided Mol. Des.* 1–9 (2021).
58. Mayr, A., Klambauer, G., Unterthiner, T. & Hochreiter, S. Deeptox: toxicity prediction using deep learning. *Front. Environ. Sci.* **3**, 80 (2016).
59. Dobson, C. M. *et al.* Chemical space and biology. *Nature* **432**, 824–828 (2004).
60. Naveja, J. J. & Medina-Franco, J. L. Finding constellations in chemical space through core analysis. *Front. Chem.* **7**, 510 (2019).
61. Stumpfe, D., Hu, H. & Bajorath, J. Evolving concept of activity cliffs. *ACS Omega* **4**, 14360–14368 (2019).
62. Deng, J. & Wang, F. An informatics-based approach to identify key pharmacological components in drug-drug interactions. *AMIA Summits on Transl. Sci. Proc.* **2020**, 142 (2020).
63. Mervin, L. H. *et al.* Probabilistic random forest improves bioactivity predictions close to the classification threshold by taking into account experimental uncertainty. *J. Cheminformatics* **13**, 1–17 (2021).
64. Truchon, J.-F. & Bayly, C. I. Evaluating virtual screening methods: good and bad metrics for the “early recognition” problem. *J. Chem. Inf. Model.* **47**, 488–508 (2007).
65. Shoichet, B. K. Virtual screening of chemical libraries. *Nature* **432**, 862–865 (2004).
66. Schisterman, E. F., Faraggi, D., Reiser, B. & Hu, J. Youden index and the optimal threshold for markers with mass at zero. *Stat Med* **27**, 297–315 (2008).
67. Cortés-Ciriano, I. & Bender, A. Kekulescope: prediction of cancer cell line sensitivity and compound potency using convolutional neural networks trained on compound images. *J. Cheminformatics* **11**, 1–16 (2019).
68. Lu, J., Deng, K., Zhang, X., Liu, G. & Guan, Y. Neural-ode for pharmacokinetics modeling and its advantage to alternative machine learning models in predicting new dosing regimens. *Iscience* **24**, 102804 (2021).
69. Sedgwick, P. A comparison of parametric and non-parametric statistical tests. *BMJ* **350** (2015).
70. Massey Jr, F. J. The kolmogorov-smirnov test for goodness of fit. *J Am Stat Assoc* **46**, 68–78 (1951).

71. Todeschini, R. *et al.* Similarity coefficients for binary chemoinformatics data: overview and extended comparison using simulated and real data sets. *J. Chem. Inf. Model.* **52**, 2884–2901 (2012).
72. Smith, M. T., Kong, D., Kuo, A., Imam, M. Z. & Williams, C. M. Analgesic opioid ligand discovery based on nonmorphinan scaffolds derived from natural sources. *J. Med. Chem* (2022).
73. Bissantz, C., Kuhn, B. & Stahl, M. A medicinal chemist's guide to molecular interactions. *J. Med. Chem* **53**, 5061–5084 (2010).
74. Hu, Y., Stumpfe, D. & Bajorath, J. Advancing the activity cliff concept. *F1000Research* **2** (2013).
75. Kolmar, S. S. & Grulke, C. M. The effect of noise on the predictive limit of qsar models. *J. Cheminformatics* **13**, 1–19 (2021).
76. Cortes-Ciriano, I., Bender, A. & Malliavin, T. E. Comparing the influence of simulated experimental errors on 12 machine learning algorithms in bioactivity modeling using 12 diverse data sets. *J. chemical information modeling* **55**, 1413–1425 (2015).
77. Deng, J., Yang, Z., Li, Y., Samaras, D. & Wang, F. Towards better opioid antagonists using deep reinforcement learning. *arXiv preprint arXiv:2004.04768* (2020).
78. Jing, L. & Tian, Y. Self-supervised visual feature learning with deep neural networks: A survey. *IEEE PAMI* **43**, 4037–4058 (2020).
79. Liu, X. *et al.* Self-supervised learning: Generative or contrastive. *arXiv preprint arXiv:2006.08218* **1** (2020).
80. Lane, T. R. *et al.* Bioactivity comparison across multiple machine learning algorithms using over 5000 datasets for drug discovery. *Mol. Pharm.* **18**, 403–415 (2020).
81. Walters, W. P. & Murcko, M. Assessing the impact of generative ai on medicinal chemistry. *Nat. Biotechnol.* **38**, 143–145 (2020).
82. Bender, A. *et al.* Evaluation guidelines for machine learning tools in the chemical sciences. *Nat. Rev. Chem.* 1–15 (2022).
83. Deng, J. *et al.* A review of food–drug interactions on oral drug absorption. *Drugs* **77**, 1833–1855 (2017).
84. Fort, S., Hu, H. & Lakshminarayanan, B. Deep ensembles: A loss landscape perspective. *arXiv preprint arXiv:1912.02757* (2019).
85. Jiménez-Luna, J., Grisoni, F. & Schneider, G. Drug discovery with explainable artificial intelligence. *Nat. Mach. Intell.* **2**, 573–584 (2020).

Acknowledgements

The experiments in this study are conducted using the computational resources provided by the AI Institute in Stony Brook

University. The authors also want to acknowledge the explicit codes and pretrained models from MolBERT and GROVER.

Author contributions statement

J.D. and Z.Y. conceived and designed the study. J.D. collected the datasets, conducted the experiments and analyzed the results. J.D. wrote the first draft of the manuscript. H. W. curated the chemistry-related contents. I. O., D.S. and F.W. supervised the project. F. W. provided funding support. All authors proofread the manuscript and made critical revisions.

Additional information

Accession codes The code, data and raw results are available in the Github repository: https://github.com/dengjianyuan/Respice_MPP. **Competing interests** The authors have no competing interest.